ISTANBUL TECHNICAL UNIVERSITY ★ GRADUATE SCHOOL

UNDERSTANDING THE DYNAMICS OF AIR POLLUTION DURING FOREST FIRES IN ANTALYA-MANAVGAT: A WRF-CHEM ANALYSIS

M.Sc. THESIS

Yiğitalp KARA

Department of Meteorological Engineering

Atmospheric Sciences Programme

JUNE 2024

ISTANBUL TECHNICAL UNIVERSITY ★ GRADUATE SCHOOL

UNDERSTANDING THE DYNAMICS OF AIR POLLUTION DURING FOREST FIRES IN ANTALYA-MANAVGAT: A WRF-CHEM ANALYSIS

M.Sc. THESIS

Yiğitalp KARA
(511221017)

Department of Meteorological Engineering

Atmospheric Sciences Programme

Thesis Advisor: Prof. Dr. Hüseyin TOROS

JUNE 2024

ISTANBUL TEKNİK ÜNİVERSİTESİ ★ LİSANSÜSTÜ EĞİTİM ENSTİTÜSÜ

ANTALYA-MANAVGAT'TA ORMAN YANGINLARINDA HAVA KİRLİLİĞİNİN DİNAMİKLERİNİ ANLAMAK: WRF-CHEM ANALİZİ

YÜKSEK LİSANS TEZİ

Yiğitalp KARA
(511221017)

Meteoroloji Mühendisliği Anabilim Dalı

Atmosfer Bilimleri Programı

Tez Danışmanı: Prof. Dr. Hüseyin TOROS

HAZİRAN 2024

Yiğitalp KARA, a M.Sc. student of ITU Graduate School student ID 511221017, successfully defended the thesis entitled “UNDERSTANDING THE DYNAMICS OF AIR POLLUTION DURING FOREST FIRES IN ANTALYA-MANAVGAT: A WRF-CHEM ANALYSIS”, which he/she prepared after fulfilling the requirements specified in the associated legislations, before the jury whose signatures are below.

Thesis Advisor :	**Prof. Dr. Hüseyin TOROS** Istanbul Technical University	....
Jury Members :	**Assist. Prof. Dr. Ceyhan KAHYA** Istanbul Technical University	....
	Assist. Prof. Dr. Veli YAVUZ Samsun University	....

Date of Submission : 09 May 2024
Date of Defense : 06 June 2024

I dedicated this to myself because without myself I couldn't have done it,

FOREWORD

Dear Esteemed Reader,

It is with great pleasure and enthusiasm that I present to you this illustrious masterpiece of academic brilliance, the thesis entitled "Understanding the Dynamics of Air Pollution During Forest Fires in Antalya-Manavgat: A WRF-CHEM Analysis." This research endeavor has been conducted as part of the requirements for the Master's program in Atmospheric Sciences at Istanbul Technical University. This thesis endeavors to delve into the intricate dynamics of air pollution during forest fires in the Antalya-Manavgat region, employing advanced modeling techniques, specifically the Weather Research and Forecasting with Chemistry (WRF-CHEM) model. Through this analysis, I aim to elucidate the complex interactions between meteorological conditions, fire dynamics, and air quality parameters during fire events.

I extend my sincere gratitude to my advisor, Prof. Dr. Hüseyin TOROS, whose guidance has been as invaluable as a compass in a dense fog. His expertise has been instrumental in shaping the direction and methodology of this study. Special thanks are due to the Turkish State Meteorological Service and the Ministry of Environment, Urbanisation, and Climate Change for their essential data and resources. Computing resources used in this work were provided by the National Center for High Performance Computing of Turkey (UHeM) under grant number <4016712023>. Because who knew you needed a supercomputer to analyze the air quality during a forest fire?

With a respectful salute to academia,

June 2024 | Yiğitalp KARA
Research Assistant

TABLE OF CONTENTS

Page

FOREWORD ix
TABLE OF CONTENTS xi
ABBREVIATIONS xiii
SYMBOLS xv
LIST OF TABLES xvii
LIST OF FIGURES xix
SUMMARY xxi
ÖZET xxv
1. INTRODUCTION 1
1.1 Purpose of Thesis 3
1.2 Literature Review 4
1.3 Case Description 5
1.4 Hypothesis 6
2. METHODS 7
2.1 Study Area 7
2.1.1 Geography 7
2.1.2 Climate 8
2.1 Data 9
2.1.3 WRF-Chem model data 9
2.1.1.1 ERA5 Reanalysis Data 9
2.1.1.2 The fire inventory from NCAR (FINN) 10
2.1.1.3 PREP-CHEM-SRC Preprocessor 11
2.2 The Goddard Chemistry Aerosol Radiation and Transport (GOCART) 11
2.3 The Emissions Database for Global Atmospheric Research (EDGAR) HTAP12
2.4 Reanalysis of the Tropospheric Chemical Composition Over the Past 40 Years project (RETRO). 13
2.5 Global Emissions InitiAtive (GEIA) 13
2.6 Logan Yevich emission 14
2.1.4 Ground measurement data 14
2.1.5 Satellite Data 15
2.6.1.1 MODIS Multi-Angle Implementation of Atmospheric Correct (MAIAC) 15
2.6.1.2 VIIRS (NOAA-20/JPSS-1) I Band 375 m Active Fire Product NRT 16
2.6.1.3 Sentinel-5P OFFL AER AI: Offline UV Aerosol Index 17
2.7 Methods 18
2.1.6 The Weather Research and Forecasting with Chemistry (WRF-CHEM). 18
2.7.1.1 The Weather Research and Forecasting Pre-Processing System (WPS) 19
2.7.1.2 Gridded Chemistry Data Input to WRF-CHEM 20
2.1.7 Configuration options of WRF-CHEM Model 20
3. RESULTS 23
3.1 Synoptic Analysis of Manavgat Forest Fire 23

3.2 Micrometeorologic Analysis of Manavgat Forest Fire 26
3.3 Geospatial Analysis of the Event 29
3.4 Hotspot Detection 30
3.5 Performance of WRF-CHEM for Meteorological Variables 31
3.6 Descriptive Statistics of Measured and Modeled Air Pollutants...................... 32
3.7 Pollution Calendars and Air Quality Index (AQI) 35
3.8 Performance of WRF-CHEM for AOD and PM_{10} 37
3.9 Performance of WRF-CHEM PM_{10} 43
3.10 Fire Plume Modelling and PM_{10} Cross Section 45
3.11 Particulate Matter Transportation Event 48
4. DISCUSSION 49
4.1 Meteorological Situation 49
4.2 PM_{10} and Aerosol Optical Depth (AOD) 50
4.3 3D Plume Modeling 51
4.4 Transportation Event 52
5. CONCLUSIONS AND RECOMMENDATIONS 53
5.1 Meteorological Influence on Fire Behavior 53
5.2 Performance of WRF-Chem Model 54
5.3 Discrepancy Analysis through 3D Fire Plume Modeling................................. 55
6. REFERENCES 57
7. CURRICULUM VITAE 65

ABBREVIATIONS

AAI	: Aerosol Absorption Index
AOD	: Aerosol Optical Depth
ASEAN	: Association of Southeast Asian Nations
BAI	: Burned Area Index
BC	: Black Carbon
BLPC	: Basra Low-Pressure Center
CH_4	: Methane
CO	: Carbon Monoxide
CO_2	: Carbon Dioxide
CPTEC/INPE	: Center for Weather Forecasting and Climate Studies/National Institute for Space Research
dNBR	: Difference Normalized Burned Ratio Index
dNDVI	: Difference Normalized Difference Vegetation Index
ECMWF ERA5	: European Centre for Medium-Range Weather Forecasts Fifth Generation Reanalysis
EDGAR HTAP	: Emissions Database for Global Atmospheric Research Hemispheric Transport of Air Pollution
EDGAR	: Emissions Database for Global Atmospheric Research
EEA	: European Environment Agency
EMEP/TNO	: European Monitoring and Evaluation Programme/TNO
ERA5	: ECMWF's fifth-generation reanalysis
ESA	: European Space Agency
FINNv2.5	: Fire INventory from NCAR version 2.5
GEIA	: Global Emissions InitiAtive
GOCART	: Goddard Chemistry Aerosol Radiation and Transport
GRIB	: Gridded Binary
HTAP	: Hemispheric Transport of Air Pollution
JPSS	: Joint Polar Satellite System
MAIAC	: Multi-Angle Implementation of Atmospheric Correction
MICS-Asia	: Model Inter-Comparison Study for Asia
MODIS	: Moderate Resolution Imaging Spectroradiometer

MYJ	: Mellor-Yamada-Janjic
NCAR	: National Center for Atmospheric Research
NDVI	: Normalized Difference Vegetation Index
NMVOC	: Non-Methane Volatile Organic Compounds
NO_2	: Nitrogen Dioxide
NOAA	: National Oceanic and Atmospheric Administration
Noah-MP	: Noah Multi-Physics NOx: Nitrogen Oxides
OC	: Organic Carbon
PM_{10}	: Particulate Matter
$PM_{2.5}$	: Particulate Matter with a diameter of 2.5 micrometers or less
PREP-CHEM-SRC	: Emissions Pre-Processor for Chemistry
RACM-KPP	: Regional Atmospheric Chemistry Mechanism-Kinetic PreProcessor
REAS	: Regional Emission inventory in Asia
RETRO	: REmote sensing TRANsport of pollutants
RRTMG	: Rapid Radiative Transfer Model for General Circulation Models
SAVI	: Soil-Adjusted Vegetation Index
SO_2	: Sulfur Dioxide
SST	: Sea Surface Temperature
TROPOMI	: TROPOspheric Monitoring Instrument
US-EPA	: United States Environmental Protection Agency
UVAI	: Ultraviolet Aerosol Index
VIIRS	: Visible Infrared Imaging Radiometer Suite
WPS	: WRF Pre-Processing System
WRF-Chem	: Weather Research and Forecasting with Chemistry
WSM6	**:** Weather Research and Forecasting model's 6th generation Weather Research and Forecasting Single-Moment Microphysics Scheme

SYMBOLS

°C	: Celcius degree
R	: Pearson correlation coefficient
µg/m³	: Micrograms per cubic meter

LIST OF TABLES

Page

Table 2.1 : Climate Classification of Antalya (Klimatoloji Şube Müdürlüğü, 2014). 9
Table 2.2 : Measured pollutants by AQI station in Antalya 15
Table 2.3 : Configuration options of WRF-CHEM Model. 21
Table 3.1 : Important dates of Antalya Manavgat forest fire disaster. 30
Table 3.2 : Descriptive Statistics of observed and modeled PM_{10} 33
Table 3.3 : Air Quality Index (AQI) Categories Based on 24-Hour Mean PM_{10} Concentration 35
Table 3.4 : AOD and AAI time series of four station grids. 41

LIST OF FIGURES

Page

Figure 2.1 : Map of Antalya ... 7
Figure 2.2 : FINN PM_{10} Data on the date of the fire initation (29.07.2023) ... 11
Figure 2.3 : EDGAR HTAP PM_{10} Sources of 2010 (Janssens-Maenhout et al., 2015) ... 12
Figure 2.4 : Air quality stations in Antalya over MODIS surface reflectance band 1 (620-670 nm) imagery on 29.07.2021 ... 15
Figure 2.5 : MCD19A2 dataset with 0.47nm optical depth imagery on 29.07.2021 16
Figure 2.6 : The VIIRS (Visible Infrared Imaging Radiometer Suite) Fire and Thermal Anomalies (Day, 375m) Imagery on 28.07.2023 ... 17
Figure 2.7 : Sentinel-5P OFFL AER AI: Offline UV Aerosol Index Imagery on 28.07.2023 ... 18
Figure 2.8 : Diagram of WRF-Chem processes ... 19
Figure 3.1 : Synoptic composite charts during fire event. ... 25
Figure 3.2 : 3D Wind trajectory visualization over the Toros Mountains indicating Foehn wind patterns (above) surface weather chart (middle), time-series of observed and WRF-Chem meteorological variables (below). ... 28
Figure 3.3 : Visualization of both model and satellite observations on important dates of Antalya Manavgat forest fire disaster. ... 29
Figure 3.4 : Comparative Analysis of Forest Fire Hotspots: WRF-Chem (Left) vs. VIIRS (Right). ... 30
Figure 3.5 : Taylor diagrams of meteorological variables. ... 32
Figure 3.6 : Boxplot of observed and modeled PM_{10} ... 34
Figure 3.7 : Histogram of observed and modeled PM_{10} ... 34
Figure 3.8 : Pollution calendars of Muratpaşa, Serik, Manavgat, and Alanya stations, respectively, colorized according to EPA AQI classification. ... 36
Figure 3.9 : Spatial Distribution of AOD and AAI from WRF-CHEM, MAIAC, NRTI AER AI. ... 38
Figure 3.10 : Normalized Time series of AOD and AAI (left) and correlation matrices with dendogram (right). ... 42
Figure 3.11 : Time series and scatter plot with a density overlay of observed and modeled PM_{10}. ... 45
Figure 3.12 : 3D fire plume modeling with wind trajectories (right), cross section of plume with PM_{10} quantities (left). ... 47
Figure 3.13 : Aqua Modis Corrected reflectance imagery on 05.08.2021 and 06.08.202. ... 48

UNDERSTANDING THE DYNAMICS OF AIR POLLUTION DURING FOREST FIRES IN ANTALYA-MANAVGAT: A WRF-CHEM ANALYSIS

SUMMARY

This thesis aims to investigate the air pollution dynamics of the Antalya Manavgat forest fires in Turkey, utilizing the advanced Weather Research and Forecasting model coupled with Chemistry (WRF-Chem) and the Fire INventory from NCAR version 2.5 (FINN v2.5) boundary fire emission data. The research is dedicated to comprehensively understanding both the synoptic and microscale atmospheric conditions that prevailed during the forest fire events, delving into the complexities of meteorological influences on fire behavior and pollutant distribution. A key aspect of our investigation is examining the influence of the Foehn effect, a dry and warm down-slope wind, on intensifying the initial fire conditions which may exacerbate fire spread and severity. This phenomenon is critical as it can significantly modify the local weather conditions and thereby affect the behavior of the fire and the resultant air quality issues. Furthermore, the thesis rigorously assesses the performance of the WRF-Chem model in accurately predicting essential atmospheric parameters such as Aerosol Optical Depth (AOD), Aerosol Absorption Index (AAI), Particulate Matter (PM_{10}), and various meteorological variables. The analysis of atmospheric conditions during the Manavgat forest fires in Antalya between July 26 and August 9, 2021, revealed several key findings.

The Weather Research and Forecasting model coupled with Chemistry (WRF-Chem) is a state-of-the-art atmospheric modeling system utilized for simulating the interactions between meteorology and atmospheric chemistry. With options for two domains, spanning varying resolutions from 9×9 km to 3×3 km, and employing 50 vertical levels, WRF-Chem offers detailed insights into atmospheric processes. Meteorological boundary conditions are derived from ECMWF ERA5 Reanalysis data, supplemented by sea surface temperature data from the same source. Cloud microphysics are parameterized using the WSM6 scheme, while boundary layer dynamics are modeled using the MYJ scheme. The representation of cumulus clouds follows the Grell-3 scheme, and radiative processes are accounted for with the RRTMG scheme for both longwave and shortwave radiation. The land surface is modeled using the Noah-MP scheme, while the surface layer incorporates the Eta Similarity scheme. Chemically, WRF-Chem employs the GOCART scheme coupled with RACM-KPP for simulating atmospheric chemistry, facilitating the study of aerosol-radiation interactions and chemical transport processes. Additionally, it integrates various emissions databases like the NCAR Fire INventory from NCAR (FINN), PREP-CHEM-SRC Preprocessor, EDGAR HTAP, RETRO, GEIA, and Logan Yevich emissions, enabling comprehensive investigations into global atmospheric composition and pollutant distributions over time.

The synoptic composite charts provided insights into the prevailing meso- or synoptic-scale structures during the fire event. At the 1000 hPa level, the influence of the Basra Low-Pressure Center (BLPC) was observed, which transported dry and warm air into the region via easterly flows. The 850 hPa level showed a low-pressure center above the BLPC, contributing to dry and warm air reaching the Manavgat district. At the 700 hPa level, dry and warm air persisted, limiting convective activities and rainfall. Micrometeorological analysis, using the Weather Research and Forecasting (WRF) model, examined the connection between large-scale atmospheric conditions and surface-level meteorological phenomena. The WRF model provided high-resolution outputs of temperature and relative humidity, which are crucial for understanding fire behavior. Factors such as high temperatures, low relative humidity, scarce precipitation, and local wind characteristics were identified as significant contributors to fire risks. The Foehn effect, characterized by warm and arid winds resulting from adiabatic compression, was found to exacerbate fire conditions. The WRF-Chem model demonstrated how the Foehn effect influenced airflow patterns over the Toros Mountains, leading to warming and drying of the air on the lee side, which heightened fire risks. Surface weather charts and temperature and humidity measurements confirmed the presence of the Foehn effect during the initial days of the fire, with high temperatures and low relative humidity.

The performance of the WRF-Chem model for various meteorological variables was evaluated using correlation coefficient analysis across different observed locations. Taylor diagrams for the meteorological variables show that temperature exhibited strong positive relationships across all observed locations, with high correlation coefficients. Kepez had the highest correlation coefficient of 0.94, followed closely by Muratpasa (0.84), Kumluca (0.91), Manavgat (0.84), Alanya (0.82), Serik (0.58), and Gazipasa (0.62). These high coefficients indicate a consistent agreement between temperature measurements or model outputs and the reference data in these regions. Relative humidity also demonstrated solid positive correlations in most stations. The strongest correlations were observed in Alanya (0.80) and Manavgat (0.80), followed closely by Muratpasa (0.74), Gazipasa (0.64), Kumluca (0.68), Kepez (0.55), and Serik (0.38). This suggests that the model effectively captured the variations in humidity in these areas. Wind speed correlations exhibited more variability. Muratpasa showed a strong positive correlation (0.61), followed by Manavgat (0.62), Kumluca (0.49), Gazipasa (0.48), Alanya (0.40), Kepez (0.33), and Serik with a notably lower correlation (0.06). On the other hand, atmospheric pressure correlation coefficients were consistently high across all reported locations, indicating excellent agreement with the reference data. Muratpasa demonstrated exceptional correlation (0.95), with Gazipasa also exhibiting a very high correlation (0.95). Manavgat (0.94) and Serik (0.51) also showed strong correlations. This suggests that pressure data from these locations aligned very well with the reference dataset. Overall, Muratpasa and Manavgat stood out as locations with high correlations across all meteorological variables, indicating a strong agreement between model outputs or measurements for these specific sites.

Understanding the interplay between AOD measurements from satellite observations, such as MAIAC AOD, and those derived from atmospheric models like WRF-Chem AOD, aerosol absorption indices AAI such as AER AAI, provides crucial insights into the accuracy and reliability of aerosol characterization methodologies. At the Muratpaşa Station, the strong positive correlation (r = 0.94) between MAIAC AOD and WRF-Chem AOD data underscores the close alignment of the model with satellite observations, highlighting its accuracy in capturing aerosol concentrations. However, the moderate correlations with AER AAI data ($r = 0.45$ with WRF-Chem AOD and $r = 0.35$ with MAIAC AOD) suggest discrepancies in aerosol property measurements from different sources, reflecting the complexity of aerosol characterization. Contrarily, the Serik Station's findings reveal diminished correlations, with a moderate correlation coefficient of 0.41 between MAIAC AOD and WRF-Chem AOD, hinting at significant limitations in the model's ability to depict local aerosol concentrations accurately. This is further compounded by the influence of meteorological conditions on aerosol transport, particularly evident on specific dates like August 1st. The data from Manavgat and Alanya Stations also demonstrate significant yet varying degrees of correlation: while Manavgat shows a high degree of model agreement with correlations reaching up to $r = 0.93$ with MAIAC AOD, Alanya presents robust correlations ($r = 0.80$ with MAIAC AOD) but also showcases consistency when compared with AER AAI measurements ($r = 0.71$).

This thesis also examines the performance of the WRF-Chem model in simulating ground level PM_{10} concentrations across four stations in the Antalya-Manavgat region: Muratpaşa, Serik, Manavgat, and Alanya. At Muratpaşa, a strong positive correlation ($r = 0.72$) indicates close alignment between modeled and observed PM_{10} levels, reflecting the model's ability to replicate diurnal variations. In Serik, while there is noticeable agreement, the correlation coefficient is modest ($r = 0.44$), suggesting reduced precision, due to limitations in representing local meteorological conditions. Conversely, in Manavgat, the model demonstrates remarkable accuracy, with a high correlation coefficient ($r = 0.82$), even during extreme pollution events like the Antalya Manavgat forest fires. However, at Alanya, while AOD measurements exhibit a strong correlation ($r = 0.80$), ground-level PM_{10} predictions show divergence, with a moderate positive correlation ($r = 0.50$), highlighting the need for refinement in representing aerosol dynamics at lower altitudes. The observed discrepancies underscore the necessity of exploring atmospheric pollutant dispersion dynamics through 3D fire plume modeling and wind trajectory analysis to enhance model accuracy in assessing air quality impacts.

To explore the discrepancies between modeled and observed pollutant concentrations, the thesis employs 3D fire plume modeling, wind trajectories, and PM_{10} cross-sectional data. The analysis aims to capture the vertical and horizontal movement of pollutants emitted from the forest fire source. Thermal updrafts induced by the intense heat of the fire play a crucial role in the vertical dispersion of PM_{10} particles. As temperatures decrease, the uplifted particles disperse horizontally within the atmosphere, potentially influencing air quality at upper atmospheric levels. However, air movements can lead to the descent of PM_{10} particles to the ground, resulting in elevated particulate matter concentrations near the surface. The thesis also highlights the complex dynamics of wildfire smoke and particulate matter transport. Even after the cessation of local fires, particulate matter, including PM_{10} particles, can originate from remote sources (Greece) and near sources (Muğla) is conveyed across the region by atmospheric currents. The transport of smoke and aerosols over vast distances can significantly impact local air quality. By integrating synoptic maps with advanced 3D modeling techniques, the thesis reveals that the fire plume reaches impressive altitudes of up to 6 kilometers above sea level. This elevation is influenced not only by thermal effects but also by the presence of a dynamic low-pressure system in the atmosphere.

ANTALYA-MANAVGAT'TAKİ ORMAN YANGINLARINDA HAVA KİRLİLİĞİNİN DİNAMİKLERİNİ ANLAMAK: WRF-CHEM ANALİZİ

ÖZET

Bu tez, Türkiye'deki Antalya Manavgat orman yangınlarının hava kirliliği dinamiklerini Weather Research and Forecasting with Chemistry (WRF-Chem) ve NCAR v2.5 (FINN v2.5) yangın emisyon envanterini kullanarak araştırmayı amaçlamaktadır. Araştırmanın odak noktası, Fön etkisinin yangın koşullarını nasıl yoğunlaştırdığını ve bu durumun yangın yayılmasını ve şiddetini nasıl artırabileceğini incelemektir. Bu etki yerel hava koşullarını önemli ölçüde değiştirmiş ve dolayısıyla yangının davranışını ve bunun sonucunda ortaya çıkan hava kalitesini etkilemiştir. Dahası, çalışma, WRF-Chem modelinin, Aerosol Optik Derinlik (AOD), Aerosol Absorpsiyon İndeksi (AAI), Partikül Madde (PM_{10}) ve çeşitli meteorolojik değişkenler gibi temel atmosferik parametreleri doğru bir şekilde tahmin etmedeki performansını titizlikle değerlendirmektedir. 2021 yılı 26 Temmuz ile 9 Ağustos tarihleri arasındaki Antalya Manavgat orman yangınları sırasındaki atmosferik koşulların analizi çeşitli önemli bulgular ortaya koymuştur.

Weather Research and Forecasting with Chemistry (WRF-Chem), meteoroloji ile atmosfer kimyası arasındaki etkileşimleri simüle etmek için kullanılan son teknoloji bir atmosferik modelleme sistemidir. Tezde, 9×9 km ile 3×3 km çözünürlüklerde iki domain kullanılmıştır. 50 dikey seviye kullanarak ayrıntılı bir şekilde atmosferik süreçlere ışık tutan WRF-Chem'in, meteorolojik sınır koşulları ECMWF ERA5 Reanaliz verilerinden türetilmiş olup, aynı kaynaktan deniz yüzeyi sıcaklık verileri ile desteklenmektedir. Bulut mikrofiziği, WSM6 şeması kullanılarak parametrelendirilirken, sınır tabakası dinamikleri MYJ şeması ile modellenmektedir. Kümülonimbus bulutlarının temsili Grell-3 şemasını izlerken, radyatif süreçler uzun dalga ve kısa dalga radyasyon için RRTMG şeması ile hesaplanmaktadır. Arazi yüzeyi Noah-MP şeması kullanılarak modellenirken, yüzey tabakası Eta Benzerlik şemasını içermektedir. Kimyasal olarak, WRF-Chem'de, atmosfer kimyasını simüle etmek için GOCART şemasını ve aerosol-radyasyon etkileşimlerini ve kimyasal taşıma süreçlerini incelemeyi kolaylaştıran RACM-KPP ile birleştirilmiş bir yapı kullanılmıştır. Ayrıca, NCAR Fire INventory from NCAR (FINN), PREP-CHEM-SRC Ön İşlemci, EDGAR HTAP, RETRO, GEIA ve Logan Yevich emisyonları gibi çeşitli emisyon veritabanlarını entegre ederek, zaman içinde geniş kapsamlı atmosferik kompozisyon ve kirletici dağılımlarının detaylı olarak incelenmesini sağlanmıştır.

Sinoptik haritalar, yangın olayı sırasında hakim olan orta ve sinoptik ölçekli yapılara ilişkin bilgiler sağlamıştır. 1000 hPa düzeyinde ise kuru ve sıcak havayı doğu yönlü akışlarla bölgeye taşıyan Basra Alçak Basınç Merkezi'nin (BLPC) etkisi gözlemlenmiştir. 850 hPa seviyesinde BLPC'nin üzerinde bir alçak basınç merkezi bulunmakta olup, bu durum kuru ve sıcak havanın Manavgat ilçesine ulaşmasına sebep olmuştur. 700 hPa seviyesinde kuru ve sıcak hava edip ve konvektif faaliyetleri ve yağışları sınırlamıştır. Weather Research and Forecasting (WRF) modelini kullanılarak yapılan mikrometeorolojik analiz, büyük ölçekli atmosferik koşullar ile

yüzey seviyesindeki meteorolojik olaylar arasındaki bağlantıyı çözmeye yardımcı olmuştur. WRF modeli, yangın davranışını anlamak için çok önemli olan yüksek çözünürlüklü sıcaklık ve bağıl nem çıktıları sağlamıştır. Yüksek sıcaklıklar, düşük bağıl nem, az yağış ve yerel rüzgar özellikleri gibi faktörlerin, yangın risklerine önemli katkıda bulunan faktörler olduğu belirlenmiştir. Adyabatik sıkıştırmadan kaynaklanan sıcak ve kurak rüzgarlarla karakterize edilen Foehn etkisinin, yangın koşullarını kötüleştirdiği tespit edilmiştir. WRF-Chem modeli, Foehn etkisinin Toros Dağları üzerindeki hava akışı düzenlerini nasıl etkilediğini, rüzgar altı tarafta (lee-side) havanın ısınmasına ve kurumasına yol açarak yangın risklerini nasıl artırdığını göstermiştir. Yüzey haritaları, sıcaklık ve nem ölçümleri, yangının ilk günlerinde yüksek sıcaklıklar ve düşük bağıl nem ile Foehn etkisinin varlığını doğrulamıştır.

WRF-Chem modelinin çeşitli meteorolojik değişkenler için performansı, farklı gözlem noktalarında korelasyon analizi kullanılarak değerlendirilmiştir. Meteorolojik değişkenler için Taylor diyagramları, sıcaklığın tüm gözlem noktalarında yüksek korelasyon katsayıları ile güçlü pozitif ilişkiler gösterdiğini göstermektedir. Kepez en yüksek korelasyon katsayısına (0.94) sahip olup, onu yakından takip eden Muratpaşa (0.84), Kumluca (0.91), Manavgat (0.84), Alanya (0.82), Serik (0.58) ve Gazipaşa (0.62) bulunmaktadır. Bu yüksek katsayılar, bu bölgelerde sıcaklık ölçümleri veya model çıktıları ile referans verileri arasında tutarlı bir uyum olduğunu göstermektedir. Bağıl nem de çoğu istasyonda sağlam pozitif korelasyonlar gösterdi. En güçlü korelasyonlar Alanya'da (0.80) ve Manavgat'ta (0.80) gözlemlenmiş olup, onları yakından takip eden Muratpaşa (0.74), Gazipaşa (0.64), Kumluca (0.68), Kepez (0.55) ve Serik (0.38) geldi. Bu, modelin bu bölgelerde nemdeki değişimleri etkili bir şekilde yakaladığını göstermektedir. Rüzgar hızı korelasyonları çok daha fazla değişkenlik göstermiştir. Muratpaşa güçlü pozitif bir korelasyon (0.61) görülürken onu Manavgat (0.62), Kumluca (0.49), Gazipaşa (0.48), Alanya (0.40), Kepez (0.33) ve özellikle çok düşük bir korelasyon ile Serik (0.06) izledi. Diğer yandan, atmosferik basınç korelasyon katsayıları tüm analiz yapılan konumlar için yüksekti, bu da referans verilerle mükemmel bir uyumu göstermektedir. Muratpaşa olağanüstü bir korelasyon (0.95) ve Gazipaşa da çok yüksek bir korelasyon sergiledi (0.95). Manavgat (0.94) ve Serik (0.51) de güçlü korelasyonlar gösterdi. Bu, bu konumlardan basınç verilerinin ölçümlerle ile çok iyi uyum sağladığını göstermektedir. Genel olarak, Muratpasa ve Manavgat, tüm meteorolojik değişkenler arasında yüksek korelasyona sahip lokasyonlar olarak göze çarpmaktadır; bu durum, bu spesifik ölçüm lokasyonları için model çıktıları veya ölçümler arasındaki yüksek tutarlılığa işaret etmektedir.

MAIAC AOD gibi uydu gözlemlerinden elde edilen AOD ölçümleri ile WRF-Chem AOD gibi atmosferik modellerden elde edilenler ve AER AAI gibi aerosol absorpsiyon endeksleri arasındaki etkileşimin anlaşılması, aerosol karakterizasyon metodolojilerinin doğruluğu ve güvenilirliği hakkında önemli bilgiler sağlamaktadır. Muratpaşa İstasyonu'nda MAIAC AOD ve WRF-Chem AOD verileri arasındaki güçlü pozitif korelasyon (r = 0,94), modelin uydu gözlemleriyle yakın uyumunu göstermiş, aerosol konsantrasyonlarını yakalamadaki doğruluğunu vurgulamıştır. Bununla birlikte, AER AAI verileriyle orta dereceli korelasyonlar (WRF-Chem AOD ile r = 0,45 ve MAIAC AOD ile r = 0,35), farklı kaynaklardan alınan aerosol özellik ölçümlerinde aerosol karakterizasyonunun karmaşıklığını yansıtan farklılıklar olduğunu göstermektedir. Aksine, Serik İstasyonunun bulguları, MAIAC AOD ile WRF-Chem AOD arasında 0,41'lik orta düzeyde bir korelasyon katsayısı ile azalan korelasyonları ortaya koymakta olup bu da modelin yerel aerosol konsantrasyonlarını doğru şekilde gösterme yeteneğindeki önemli sınırlamalara işaret etmektedir. Bu durum, özellikle 1 Ağustos gibi belirli tarihlerde meteorolojik koşulların aerosol taşınması üzerindeki etkisi ile daha da şiddetlenmektedir. Manavgat ve Alanya İstasyonlarından elde edilen veriler de önemli ancak değişen derecelerde korelasyon göstermektedir: Manavgat, MAIAC AOD ile r = 0,93'e varan korelasyonlarla yüksek derecede model uyumu gösterirken, Alanya sağlam korelasyonlar sunmaktadır (MAIAC AOD ile r = 0,80), ancak aynı zamanda AER AAI ölçümleriyle karşılaştırıldığında da tutarlılık göstermektedir (r = 0,71).

Bu tez ayrıca Antalya-Manavgat bölgesindeki dört istasyonda (Muratpaşa, Serik, Manavgat ve Alanya) yer seviyesi PM_{10} konsantrasyonlarını simüle etme konusundaki WRF-Chem modelinin performansını da incelemektedir. Muratpaşa'da, güçlü pozitif bir korelasyon (r = 0.72), modelin gözlemlenen PM_{10} seviyeleri ile yakın uyum içinde olduğunu gösterirken, günlük değişimleri (di-urnal variation) taklit etme yeteneğini yansıtmıştır. Serik'te gözle görülür bir uyum olsa da korelasyon katsayısı ortalama düzeydedir (r = 0,44), bu durum yerel meteorolojik koşulların temsil edilmesindeki sınırlamalar nedeniyle hassasiyetin azaldığını göstermektedir. Bunun aksine, Manavgat'ta model hatta Antalya Manavgat orman yangınları gibi aşırı kirlilik olayları sırasında bile dikkate değer bir doğruluk sergilemiş, yüksek bir korelasyon katsayısı (r = 0.82) göstermiştir.. Ancak, Alanya'da, AOD ölçümleri güçlü bir korelasyon sergilese de (r = 0.80), yer seviyesi PM_{10} tahminleri ortalama bir pozitif korelasyon (r = 0.50) göstermektedir. Bu sonuç, aerosol dinamiklerinin daha yere yakın seviyede temsil edilmesinde iyileştirme ihtiyacını vurgulamaktadır. Gözlemlenen tutarsızlıklar, hava kalitesi etkilerinin değerlendirilmesinde model doğruluğunu artırmak için 3 boyutlu yangın bulutu modellemesi ve rüzgar yörünge analizi yoluyla atmosferik kirletici madde dağılım dinamiklerinin araştırılmasının gerekliliğinin altını çizmektedir.

Modellenen ve gözlemlenen kirletici konsantrasyonları arasındaki farklılıkları araştırmak için tezde 3 boyutlu yangın bulutu modellemesi, rüzgar yörüngeleri ve PM_{10} kesit verileri kullanılmıştır. Analiz, orman yangını kaynağından yayılan kirleticilerin dikey ve yatay hareketini yakalamayı amaçlamaktadır. Yangının yoğun ısısının neden olduğu termal yukarı hareketler, PM_{10} parçacıklarının dikey dağılımında çok önemli bir rol oynamaktadır. Sıcaklıklar düştükçe yükselen parçacıklar atmosferde yatay olarak dağılır ve potansiyel olarak üst atmosfer seviyelerindeki hava kalitesini de etkiler. Bununla birlikte, hava hareketleri PM_{10} parçacıklarının yere inmesine neden olabilir ve bu da yüzeye yakın parçacık madde konsantrasyonlarının artmasına neden olabilir. Tez aynı zamanda orman yangını dumanının ve partikül madde taşınmasının karmaşık dinamiklerini de vurgulamaktadır. Yerel yangınların sona ermesinden sonra bile, PM_{10} da dahil olmak üzere partiküler maddeler uzak kaynaklardan (Yunanistan) ve yakın kaynaklardan (Muğla) atmosferik akımlarla bölge boyunca taşınmıştır. Duman ve aerosollerin geniş mesafelere taşınması yerel hava kalitesini önemli ölçüde etkilemiştir. Sinoptik haritaları gelişmiş 3 boyutlu modelleme teknikleriyle birleştiren tez, yangın dumanının deniz seviyesinden 6 kilometre yüksekliğe kadar etkileyici yüksekliklere ulaştığını ortaya koymaktadır. Bu yükseklik termal etkilerin yanında aynı zamanda atmosferdeki dinamik bir alçak basınç sisteminin varlığından da etkilendiği saptanmıştır.

1. INTRODUCTION

Air quality is a critical aspect of environmental health, impacting both the natural ecosystem and human well-being. In recent years, the world has witnessed an alarming increase in the frequency and intensity of forest fires, largely attributed to climate change, land-use practices, and other anthropogenic factors (Mozny et al., 2021; Zhuang et al., 2021 ; Morison, 2023). Investigations into the impact of climate change on large fires in southern Europe reveal that warmer and drier conditions are expected to increase burned areas significantly, with the extent of the increase depending on the level of warming. However, it is suggested that substantial benefits in mitigating the risk of these large fires in Mediterranean Europe would result from limiting global warming to well below 2°C (Turco et al., 2018). In recent years, Turkey has witnessed a significant rise in the frequency of forest fires, particularly in the provinces along its Aegean and Mediterranean coastlines. These regions are more prone to forest fires due to a combination of climatic, environmental, and forest-related factors compared to other areas in the country (Akıncı et al., 2018). These fires not only pose immediate threats to lives, property, and ecosystems but also have far-reaching consequences on air quality (Jaffe et al., 2020), atmospheric chemistry, and public health.

Air pollution is a significant environmental issue that has been linked to increased mortality rates in various parts of the world (Lelieveld et al., 2020). Numerous epidemiological studies have investigated the relationship between air pollution and mortality. These studies have provided valuable insights into the health risks associated with exposure to polluted air. The harmful effects of air pollution on human health are well-documented, and they can lead to a range of serious health conditions (Song et al., 2014; Laumbach & Kipen, 2012; Ilyas et al., 2010), ultimately contributing to premature death (Kalpana et al., 2014; WHO, 2014). In addition to causing premature mortality, air pollution also results in significant morbidity, leading to people living with various diseases attributable to air pollution exposure. This imposes both personal suffering and substantial financial burdens on the healthcare sector (Jaafar et al., 2018). For instance, in 2019, the exposure to fine particulate matter

(PM2.5) in 30 European countries contributed to a total of 175,702 years lived with disability (YLDs) due to chronic obstructive pulmonary disease (EEA, 2023).

Wildfire smoke consists of a combination of dangerous air pollutants, including but not limited to PM2.5, NO2, ozone, aromatic hydrocarbons, and lead. Beyond polluting the air with harmful substances, wildfires also have a dual effect on the climate, as they release significant amounts of carbon dioxide and other greenhouse gases into the atmosphere (WHO, 2023). Wildfires represent the second most substantial origin of fine particulate matter derived from wood smoke within the province. These fires possess the potential to considerably influence nearby air quality, visibility, and human well-being. Moreover, emissions originating from forest fires can disperse over extensive distances, exerting adverse consequences in regions far removed from the fire's origin (British Columbia. (2023). Forest fires emit a complex mixture of gases and particulate matter into the atmosphere, leading to the deterioration of air quality over affected areas. The resulting pollution can exacerbate respiratory and cardiovascular health problems, increase hospital admissions, and even lead to mortality (Analitis et al., 2012). Understanding the dynamics of air quality during forest fires is crucial for effective risk assessment, disaster management, and public health protection. Safeguarding clean air ought to be regarded as a fundamental human entitlement and aligns with several United Nations sustainable development objectives, including promoting well-being, addressing climate change, fostering sustainable urban environments, advancing clean energy practices, and safeguarding terrestrial and aquatic ecosystems (Lelieveld, 2017).

The Manavgat Forest Fires that ravaged the Antalya region in Turkey during the summer of 2021 were a stark reminder of the significant challenges posed by such events. The research (Arikan & Yildiz, 2023) uncovered a significant increase in CO levels after the Antalya Manavgat fires, signifying the release of harmful pollutants into the atmosphere. This data underscored the detrimental consequences of forest fires on air quality and the environment in the Antalya region. However, another study, which relied on ground-based measurements, suggested that air pollution primarily originates from sources like motor vehicles, industrial facilities, and thermal power plants, considering forest fires as a secondary contributor to air pollution. According to their results, the forest fires in the Antalya region in 2021 did not lead to a significantly heightened level of air pollution or adversely affect air quality (Bolat, 2022). In light of these contrasting findings, it becomes important to utilize modeling approaches, such as WRF-CHEM, to gain a more comprehensive understanding of the impact of Antalya-Manavgat forest fires on air quality and the environment.

To comprehensively address the challenges posed by forest fires and their impact on air quality, sophisticated modeling tools have emerged as invaluable resources. Among these, the Weather Research and Forecasting with Chemistry (WRF-Chem) model stands out as a versatile and widely adopted tool for simulating atmospheric processes, including the dispersion and transformation of air pollutants. By integrating meteorological and chemical processes, WRF-Chem enables researchers to simulate the spatiotemporal distribution of air pollutants during events such as forest fires, providing valuable insights into the transport, transformation, and concentration of these pollutants (Grell et al., 2005). The Weather Research and Forecasting model coupled with Chemistry (WRF-Chem) is a globally recognized and extensively employed model for regional air quality simulation. Its accuracy has been confirmed through validation against ground-based observations eg., in Asia (Jiang et al., 2008; Zhou et al., 2023) in Europe (Tucella et al., 2012; Spiridonov et al., 2019) in South America (Kumar et al., 2016) in Mediterranean (Rizza et al., 2018; Rizza et al., 2023; Bossioli et al., 2016) in Turkey (Kabatas et al., 2018; Aydınöz et al., 2014).

1.1 Purpose of Thesis

The aim of this thesis is to investigate the impact of forest fires on air quality in the Antalya region, with a specific emphasis on understanding the atmospheric processes and chemical interactions that affect air quality during and after fire events. Using the WRF-Chem model as a tool, this research aims to simulate and analyze the dispersion of pollutants and particulate matter, assess the spatial and temporal variations in air quality, and provide insights into the factors influencing air quality degradation during forest fires. The findings from this thesis aim to contribute to the development of effective air quality management strategies in fire-prone regions like Antalya.

In addition to the primary aim of modeling air quality during Antalya Manavgat forest fires using the WRF-Chem model, a secondary objective is to specifically focus on the dispersion of PM_{10} (particulate matter with a diameter of 10 micrometers or less) and its impact on air quality. PM_{10} is a critical air pollutant that can have significant health and environmental consequences, especially during forest fires. This secondary aim aims to provide a more detailed understanding of PM_{10} dispersion dynamics during these events.

1.2 Literature Review

Nuryanto (2015) employed the WRF-Chem model and the Fire Inventory from NCAR (FINN) fire emissions dataset to simulate a forest fire smoke event that transpired on March 7, 2014, in Sumatera, Indonesia. The simulations, conducted from March 6, 2014, at 12 UTC to March 9, 2014, at 00 UTC, revealed the southwestward movement of the smoke, enveloping Riau Province. Furthermore, the model successfully identified Malaysia as a significant source of the smoke, which was corroborated by satellite imagery and model outputs. These simulations accurately located the forest fire sites and depicted the smoke's dispersion. In July 2018, severe heatwaves led to two major fires in Greece's Attika region, prompting a state of emergency. Madala et al. (2020), used WRF-Chem and a source generation model to simulate the emissions of aerosol pollutants and gases from these fires, shedding light on their transport and impact on local air quality. The study effectively employed WRF-Chem and the FLAMBE source generation model to model the fires' temporal and spatial evolution in Kineta and Panteli while simulating pollutant concentrations of PM2.5 and NO2 in these areas.

Navarro-Barboza et al., (2020) examined PM_{10}'s impact on aerosol optical thickness in the central Andes of Peru during July to October 2017, focusing on peak biomass burning months. Using WRF-Chem and AERONET data, it identifies a relationship between PM_{10} levels, fire outbreaks, and AOD, with contrasting trends in October due to increased rainfall, alongside varying vertical movements affecting aerosol dispersion. Heriyanto et al., (2015) addresses the issue of transboundary haze pollution caused by forest and land fires, focusing on the ASEAN region. It utilizes the Weather Research and Forecasting with Chemistry (WRF-Chem) model to simulate the dispersion of smoke resulting from fires in Indonesia, particularly in the Pekanbaru-Sumatera region. The study's findings demonstrate the effectiveness of WRF-Chem in forecasting smoke dispersion, suggesting its potential integration into an Early Warning System for such events in Indonesia. In November 2018, the devastating Camp Fire in Northern California had a profound impact on the region's air quality.

Rooney et al. (2020) combined ground-based observations of fine particulate matter (PM2.5) with numerical simulations using the Weather Research and Forecasting model coupled with chemistry (WRF-Chem) to analyze the fire's effects. The research successfully reproduces PM2.5 levels, with a focus on downwind areas, using satellite data and highlights the significance of fire emissions, meteorological conditions, aerosol radiative effects, and various parameterizations in air pollution simulations. Arikan & Yildiz (2023) focused on the 2021 fires in Antalya-Manavgat by using High-resolution satellite images, alongside plant indices like BAI, NDVI, and SAVI, were used to assess fire extent. Satellite data also revealed carbon monoxide (CO) and ultraviolet aerosol index (UVAI) values. Climate data from 2015–2021 were considered, and emissions were correlated with air quality station data. Findings highlighted forest fires as a key cause of vegetation loss and air pollution, demonstrating the ability to detect and monitor CO and aerosol indices using remote sensing satellites. This approach could also analyze plant health, fire-affected areas, and soil conditions. The study underscored the broader impact of forest fires on ecosystems, necessitating fire control measures to protect both human health and the environment.

Yilmaz et al. (2023) investigated forest fires in the Mediterranean region of Turkey during July 28, 2021, to August 11, 2021. It used Sentinel-2 satellite images and the Google Earth Engine platform to create burn severity maps based on difference normalized burned ratio index (dNBR) and difference normalized difference vegetation index (dNDVI), revealing varying levels of severity across different districts. Analysis of normalized difference vegetation index (NDVI) time series showed significant vegetation density losses in all burned areas. Additionally, post-fire analysis using Sentinel-5P satellite data detected a notable increase in Carbon Monoxide (CO) column number densities, highlighting the environmental impact of forest fires. This research provides valuable insights into assessing forest fire severity and understanding post-fire pollutant gas dynamics, emphasizing the importance of monitoring and mitigating these environmental threats.

1.3 Case Description

On July 28, 2021, around noon, wildfires erupted in four different locations within the Manavgat district of Antalya. Approximately 60,000 hectares of forested land, some of Turkey's largest forested areas, have been severely affected. The situation involved contending with a temperature of 37 degrees Celsius, humidity levels at 14%, and winds blowing at a speed of 50 kilometers per hour. All relevant data concerning the fire's progression were available, and the prevailing conditions, including wind patterns, low humidity levels, and other factors, were contributing to the fire's expansion at that time (Antalya Valiliği, 2021).

Furthermore, the economic losses incurred, encompassing damaged homes, barns, warehouses, businesses, agricultural lands, and the loss of livestock, in 59 affected neighborhoods, are estimated to be at least 1 billion Turkish Liras ("İşte Manavgat", 2021). This calamity has left a profound impact on both the natural environment and the local economy.

Both aerial and ground firefighting efforts are underway to combat the fires. The ongoing firefighting operations involve the deployment of significant resources, including 1 aircraft, 1 unmanned aerial vehicle (UAV), 19 helicopters, 192 firefighting vehicles (arazöz), 30 heavy machinery units, 960 personnel, and 30 water supply vehicles. According to information from SAKOM (Search and Rescue Coordination Center), three individuals have tragically lost their lives in the fires, and 122 people have been affected. The Ministry of Health has dispatched 19 ambulances, 6 UMKE (National Medical Rescue Teams), and 1 mobile command vehicle to the region (AFAD, 2021).

1.4 Hypothesis

The WRF-Chem model will accurately simulate the spatiotemporal distribution of air pollutants during the Antalya Manavgat Forest Fires, with a high degree of consistency between simulated results and observed air quality data. The hypothesis is formulated based on the expectation that the WRF-Chem model, known for its ability to integrate atmospheric and chemical processes, will effectively capture the dispersion, transformation, and concentration of air pollutants resulting from the forest fires in the Antalya region. The hypothesis assumes that the model's performance will be reliable and robust, allowing for meaningful insights into the air quality dynamics during the event.

2. METHODS

2.1 Study Area

2.1.1 Geography

Antalya Province is located in the southwest of Turkey, between the longitudes of 29° 20' to 32° 35' east and latitudes of 36° 07' to 37° 29' north (Figure 2.1). It is surrounded by the Mediterranean Sea to the south and the Taurus Mountains running parallel to the sea to the north. The province shares its borders with Mersin, Konya, and Karaman to the east, Isparta and Burdur to the north, and Muğla to the west. The total area of the province is approximately 20,815 square kilometers, which corresponds to about 2.6% of Turkey's total land area (Sarı & Koçak, 2012). On average, Antalya province is characterized by its topography, with approximately 77.8% of its land being mountainous, 10.2% comprising plains, and 12% featuring rugged terrain. The province's landscape is predominantly surrounded by high mountains, with notable peaks including Mount Beydağı at 3,085 meters and Mount Akdağ at 3,075 meters, emphasizing its mountainous terrain.

Figure 2.1 : Map of Antalya

2.1.2 Climate

Antalya Province experiences two distinct climate zones. Along the coastal areas, a typical Mediterranean climate prevails, characterized by hot and dry summers and mild and rainy winters. In the inland regions, a transitional climate exists between the Mediterranean climate and the Central Anatolian climate, which is often referred to as a continental climate (Antalya İl Tarım ve Orman Müdürlüğü, 2023).

In Antalya, Turkey, different climate classification methods provide insights into its climate characteristics (Table 2.1). According to the Aydeniz Climate Classification, Antalya falls into the semi-humid category with a moderate drought coefficient of 0.60, suggesting a balanced mix of rainfall and moisture. Erinç Climate Classification identifies Antalya as having a humid climate, with a high rainfall efficiency index of 44.45, indicating ample rainfall. De Martonne Climate Classification categorizes Antalya as semi-humid with a drought index of 20.53, indicating a moderate level of dryness. According to the Trewartha Climate Classification based on the Universal Temperature Scale, Antalya experiences mild winters and very hot summers, aligning with the typical Mediterranean climate pattern. Overall, these classifications collectively describe Antalya's climate as Mediterranean, characterized by warm and dry summers, mild and rainy winters, and varying degrees of humidity and dryness. Antalya's climate is categorized as B1, B'3, s2, b'3 according to the Thornthwaite Climate Classification System, with a 53% evapotranspiration rate in the summer (Klimatoloji Şube Müdürlüğü, 2014). This classification indicates that Antalya generally has a pleasant and moderate climate but faces water shortages during the summer months. The high summer evapotranspiration rate suggests that water evaporates quickly due to warm and dry summer conditions.

Table 2.1 : Climate Classification of Antalya (Klimatoloji Şube Müdürlüğü, 2014)

Aydeniz Climate Classification	Drought Coefficient	0.60
	Climate Type	Semi-Moist
Erinç Climate Classification	Precipitation activity index	44.45
	Climate Type	Moist
De Martonne Climate Classification	Drought Coefficient	20.53
	Climate Type	Semi-Moist
Trewartha Climate Classification (According to the universal temperature scale)	Jan mean temp	9.5 °C
	June mean temp	28.2 °C
	Winter	Mild Winters,
	Summer	Very Hot Summer

2.1 Data

2.1.3 WRF-Chem model data

The Weather Research and Forecasting with Chemistry (WRF-CHEM) model requires several key inputs to simulate atmospheric chemistry and aerosol processes accurately. These inputs encompass meteorological data, including initial conditions, boundary conditions, and surface characteristics, which are typically obtained from meteorological observations or other models. Additionally, emission data, detailing the release of pollutants from various sources, is essential and is provided by emission inventories. Chemical mechanisms and reaction rates define the chemical interactions in the atmosphere, while aerosol data specifies properties like size distribution, composition, and optical characteristics. These inputs collectively enable WRF-CHEM to simulate the complex interactions between meteorology, chemistry, and aerosols in the atmosphere for a range of research and forecasting applications.

2.1.1.1 ERA5 Reanalysis Data

ERA5 represents the ECMWF's fifth-generation reanalysis project, offering a comprehensive record of global climate and weather spanning the last eight decades. Its data coverage extends from 1940 onward. Reanalysis is a process that merges model-generated data with observations gathered worldwide, creating a globally comprehensive and internally consistent dataset through the application of fundamental physical principles. This method, known as data assimilation, mirrors the approach utilized by numerical weather prediction centers. In this process, at regular intervals (e.g., every 12 hours at ECMWF), a prior forecast is combined with newly acquired observations in an optimal manner to generate a fresh, refined assessment of the atmospheric state, referred to as an analysis. This analysis serves as the basis for generating an updated and enhanced weather forecast (Hersbach et al., 2023).The reanalysis process operates similarly but at a lower spatial resolution, enabling the creation of a dataset that spans multiple decades. Unlike operational weather forecasting, reanalysis is not bound by the need for immediate forecasts. Therefore, it affords more time for the collection of observations and, when delving further into the past, facilitates the incorporation of improved versions of the original observational data. These aspects collectively contribute to the enhanced quality of the reanalysis product.

2.1.1.2 The fire inventory from NCAR (FINN)

The Fire INventory from NCAR (FINN) model offers precise, high-resolution global emission assessments originating from open burning activities (Wiedinmyer et al., 2022). These emissions have been tailor-made to furnish the requisite data for modeling atmospheric chemistry and maintaining air quality within a cohesive framework, encompassing local and global scales. What sets FINN apart is its exceptional blend of fine-grained temporal and spatial accuracy, worldwide scope, and the ability to estimate emissions for a wide array of chemical components, distinguishing it from other inventory systems (NCAR, 2023). FINN leverages satellite data to detect active fires and assess land cover. Combined with emission factors and estimated fuel quantities, this approach yields daily, finely detailed (at 1 km resolution) estimates of emissions from open burning activities (Figure 2.2). These estimates are valuable inputs for regional and global chemical transport models. In FINNv2.5, an enhanced algorithm is employed to calculate fire size by consolidating neighboring fire detections. Starting from 2012, emissions data incorporate fire detections from both MODIS and VIIRS satellite instruments. To maintain consistency for extended time series analyses or model simulations, emissions are also available for the entire period dating back to 2002, relying exclusively on MODIS fire detections (Wiedinmyer et al., 2023). The gridded FINNv2.5 emissions files for 2002-2021, with a resolution of 0.1 degrees, are available from the NCAR Research Data Archive at the following link: https://rda.ucar.edu/datasets/ds312.9/.

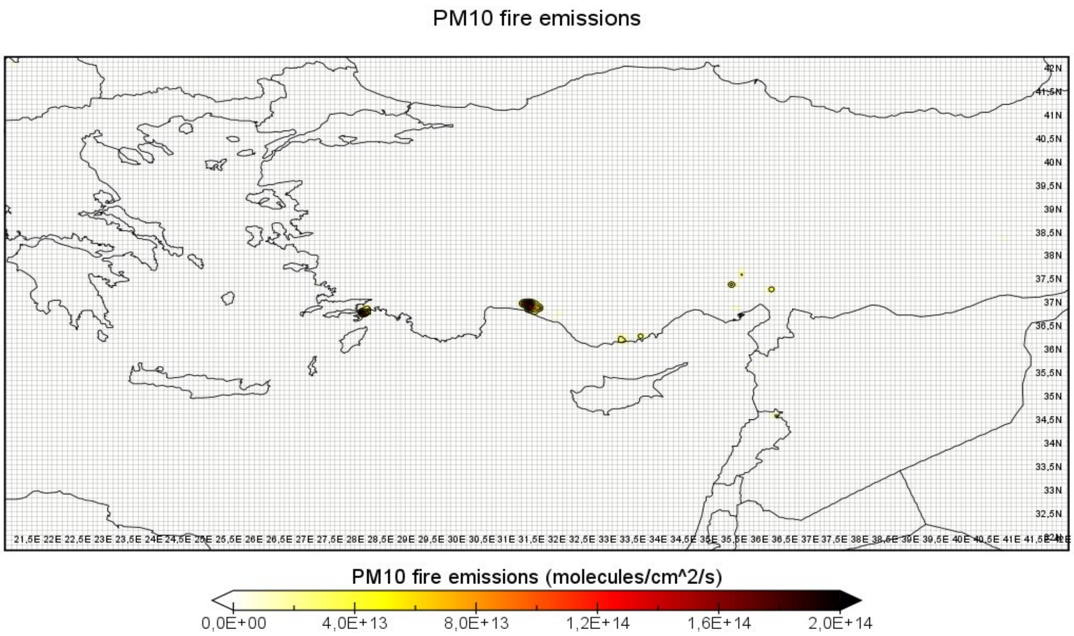

Figure 2.2 : FINN PM_{10} Data on the date of the fire initation (29.07.2023)

2.1.1.3 PREP-CHEM-SRC Preprocessor

PREP-CHEM-SRC is a computational tool for quantifying pollutant emissions, developed at CPTEC/INPE. Its primary purpose is to generate datasets of atmospheric pollutant emissions originating from a wide range of sources, including biomass burning, photosynthesis, forest transformation processes, vehicle and industrial combustion of oil-based products, charcoal production, and various other processes (Freitas et al., 2010).

2.2 The Goddard Chemistry Aerosol Radiation and Transport (GOCART)

GOCART model replicates significant aerosol constituents within the troposphere, encompassing sulfate, dust, black carbon (BC), organic carbon (OC), and sea-salt aerosols (Chin et al., 2000). This model comprises various components that emulate the release, dispersion, and settling of a wide spectrum of atmospheric aerosols, ranging from sea spray and combustion byproducts to mineral dust. The model boasts a spatial resolution spanning 2 degrees in latitude by 2.5 degrees in longitude or 1 degree by 1 degree, along with a vertical grid composed of 20 to 55 sigma layers (Ginoux et al., 2001).

2.3 The Emissions Database for Global Atmospheric Research (EDGAR) HTAP

The HTAP_V2 dataset features detailed gridmaps with a resolution of 0.1 degrees by 0.1 degrees, centered at the lower-left corner (Figure 2.3). These gridmaps provide information on various air pollutants, such as CH4, CO, SO2, NOx, NMVOC, NH3, PM_{10}, PM2.5, BC, and OC, for the years 2008 and 2010. HTAP_V2 combines nationally reported emissions data with regional scientific inventories, presented in sector-specific gridmaps. In areas where data is unavailable, EDGARv4.3 data is used to fill the gaps. This collaborative effort involves organizations like the US-EPA, MICS-Asia group, EMEP/TNO, REAS, and the EDGAR group, primarily serving the scientific community's research on air pollution transport across hemispheres (Janssens-Maenhout et al., 2015). Additionally, sectors for all substances are defined as follows: htap_1_air for international and domestic air emissions, htap_2_shipping for international shipping, htap_3_energy for power industry emissions, htap_4_industry for emissions from manufacturing, mining, metal, cement, chemical, and solvent industries, htap_5_transport for ground transport emissions (including road, rail, pipeline, and inland waterways), htap_6_residential for emissions related to heating/cooling of buildings, equipment, lighting of buildings, and waste treatment. For NH3, there is an additional sector, htap_8_agriculture, which covers emissions from agriculture but not agricultural waste burning The data is accesible from https://edgar.jrc.ec.europa.eu/dataset_htap_v2

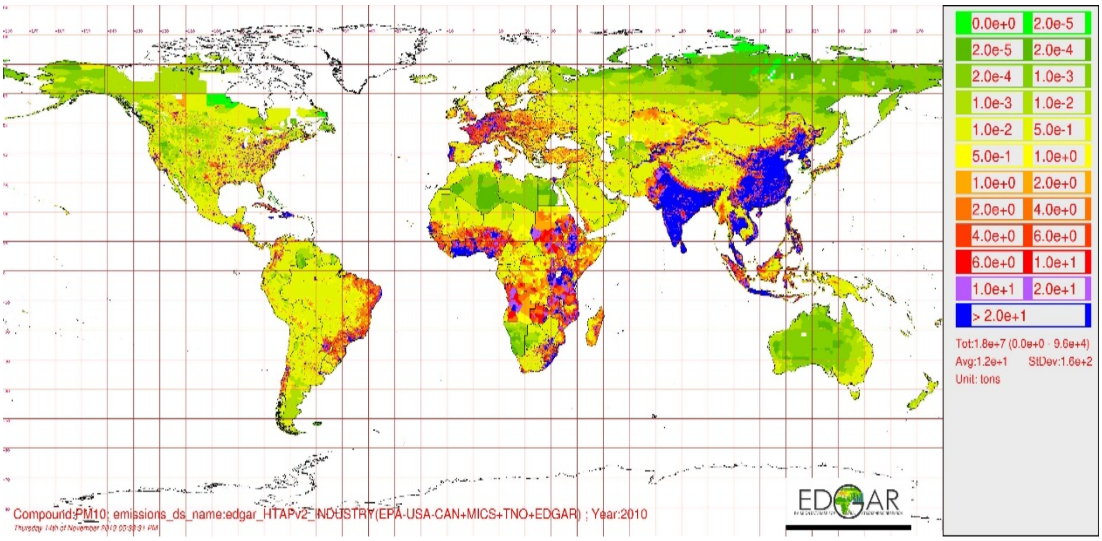

Figure 2.3 : EDGAR HTAP PM_{10} Sources of 2010 (Janssens-Maenhout et al., 2015)

2.4 Reanalysis of the Tropospheric Chemical Composition Over the Past 40 Years project (RETRO).

This paper presents a 41-year inventory of emissions from vegetation fires, developed as part of the Reanalysis of the Tropospheric Chemical Composition Over the Past 40 Years project (RETRO). RETRO is a global modeling initiative aimed at studying the long-term trends and fluctuations of tropospheric ozone and other air pollutants. Notably, this inventory represents the pioneering effort to compile a global emissions dataset with monthly temporal resolution spanning such an extensive period. To create this inventory, researchers conducted comprehensive literature reviews, analyzed various satellite datasets, and employed a numerical model that uses a semi-physical approach to simulate fire occurrences and their spread. It provides estimates for burned areas, carbon consumption, and the total release of carbon for 13 continental-scale regions (Schultz et al., 2008).

2.5 Global Emissions InitiAtive (GEIA)

The dataset provides gridded emission data with a spatial resolution of 1 degree by 1 degree, covering emissions from anthropogenic, fire, and natural sources. This dataset spans the time period from January 1990 to December 2000. Fire and natural emissions are detailed on a monthly basis, allowing for a comprehensive analysis of emissions from these sources throughout each year. In the broader context, global emissions of gases, including ozone precursors, have been assessed for the years 1990 to 2000. Anthropogenic emissions, categorized into 15 sectors, are determined based on national activity data, emission factors (measured in kg of CO per kg of fuelwood combusted per activity), and grid maps (e.g., population maps) for spatially allocating emissions within each country. For biogenic soil NOx emissions within the POET model (Granier et al., 2005), data is derived from the GEIAv1 NOx soils emissions dataset developed by Yienger and Levy in 1995. A global scaling factor is applied to ensure that the total annual emissions within the POET model align with the specified value of 8 Tg-N, while the original dataset reports emissions totaling 5.5 Tg-N. Furthermore, other biogenic emissions are estimated using a vegetation canopy model developed by S. Wallens, J.F. Muller, and A. Guenther (2008).

2.6 Logan Yevich emission

The research (Yevich & Logan, 2003) provides a comprehensive analysis of biofuel consumption and agricultural field burning practices in the developing world for the year 1985. The spatial distribution of biomass burning emissions within a 1° × 1° grid was carried out, incorporating emission factors linked to the volume of dry matter burned. This approach facilitated the creation of detailed maps illustrating trace gas emissions in the developing world. Notably, carbon monoxide (CO) emissions resulting from biofuel use in the developing world reached 156 teragrams (Tg), accounting for approximately half of the global CO emissions attributed to fossil fuel consumption and industrial processes.

2.1.4 Ground measurement data

To enhance air quality and implement effective clean air policies, the Ministry of Environment and Forestry took a significant step by establishing air quality measurement stations in all 81 provinces of Turkey between 2005 and 2007. Fast forward to 2022, and the National Air Quality Monitoring Network has achieved a remarkable milestone, now comprising a total of 360 Air Quality Monitoring Stations strategically positioned across the entire country. Accessing this invaluable data is made convenient through the official website, https://www.havaizleme.gov.tr . This web portal serves as a reliable resource for individuals, researchers, policymakers, and concerned citizens seeking real-time and historical information on a wide range of air pollutants, such as PM2.5, PM_{10}, NO2, SO2, CO, and O3. Additionally, it offers insights into air quality indices, forecasts, and interactive maps showcasing the precise locations of monitoring stations. Furthermore, the website provides educational materials, empowering the public with knowledge about the health implications of various pollutants and practical tips for minimizing exposure. In essence, this National Air Quality Monitoring Network and its accessible data are pivotal tools in the ongoing efforts to safeguard public health, drive informed policy decisions, and address environmental challenges related to air quality in Turkey. This extensive network includes 8 monitoring stations specifically in the Antalya province, all seamlessly integrated into the broader Air Quality Monitoring Network. The locations of these stations are visually represented on a map (Figure 2.4), and a comprehensive table

(Table 2.2) summarizes the various parameters measured at these sites, providing a comprehensive picture of the region's air quality.

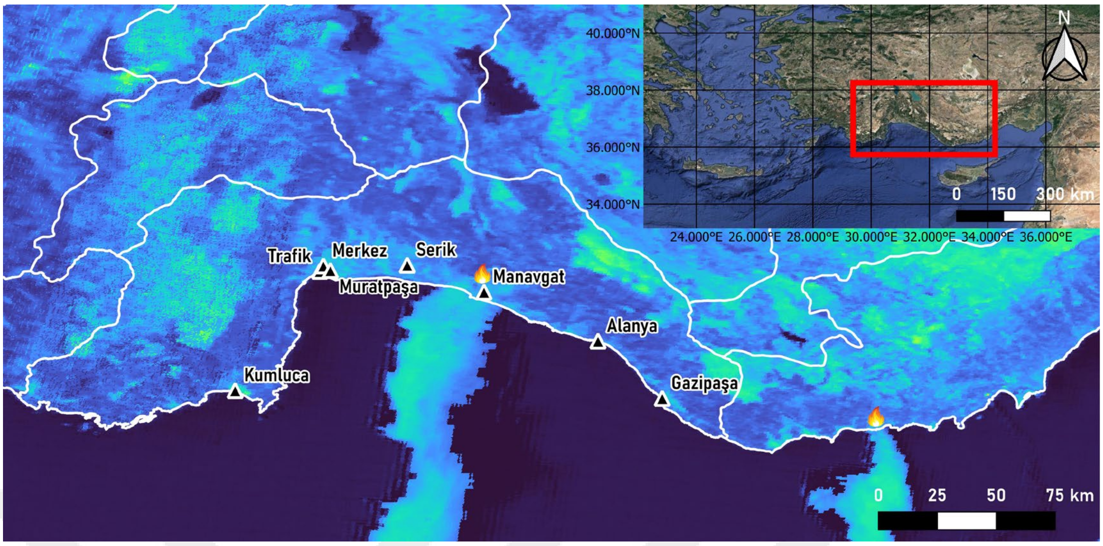

Figure 2.4 : Air quality stations in Antalya over MODIS surface reflectance band 1 (620-670 nm) imagery on 29.07.2021

Table 2.2 : Measured pollutants by AQI station in Antalya

Stations			**Pollutants**					
ID	**Name**	**Type**	PM$_{10}$	**PM2,5**	**SO2**	**NO2**	**O3**	**CO**
I	Alanya	Heating	✓			✓		
2	Manavgat	Heating	✓		✓	✓	✓	
3	Muratpaşa	Heating	✓		✓	✓		
4	Serik	Heating	✓		✓	✓		✓

2.1.5 Satellite Data

2.6.1.1 MODIS Multi-Angle Implementation of Atmospheric Correct (MAIAC)

MAIAC is renowned for its comprehensive suite of atmospheric and land surface products, which are distinguished by their exceptional cloud and snow detection capabilities and their consistent derivation from MODIS observations, adhering to the principle of energy conservation (Lyapustin & Wang, 2022). Among the atmospheric parameters provided by MAIAC are Aerosol Optical Depth (AOD), column water vapor content, and smoke injection height, all presented at a 1 km spatial resolution (Figure 2.5). MCD19A2 (Lyapustin, 2015) is the abbreviated term for the Level-2 gridded aerosol optical thickness over land surfaces product, which is based on the Multi-Angle Implementation of Atmospheric Correction (MAIAC) algorithm. This product is generated using data from both the Terra and Aqua MODIS satellites and is updated daily with a pixel resolution of 1 km. Its primary function is to compute a range of atmospheric and geometric characteristics, all of which contribute to another aspect of the MAIAC algorithm: the Bidirectional Reflectance Factor over land surfaces.

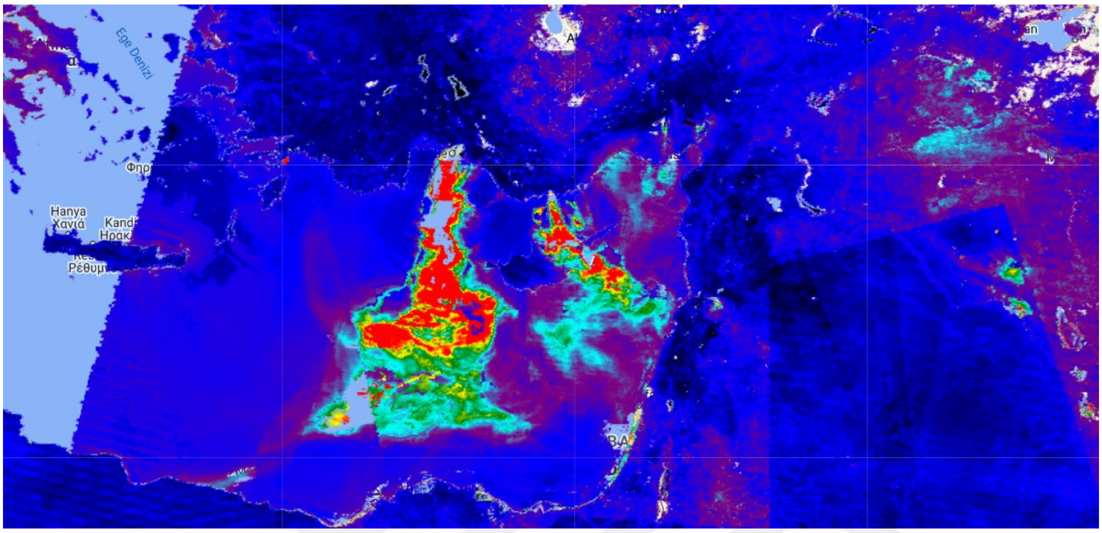

Figure 2.5 : MCD19A2 dataset with 0.47nm optical depth imagery on 29.07.2021

2.6.1.2 VIIRS (NOAA-20/JPSS-1) I Band 375 m Active Fire Product NRT

The VIIRS (Visible Infrared Imaging Radiometer Suite) Fire and Thermal Anomalies layer offers detailed insights into active fires and thermal irregularities, operating day and night with a high spatial resolution of 375 meters. These anomalies encompass various phenomena, including wildfires, volcanic eruptions, and gas flares, which can occur naturally through events like lightning strikes or result from human activities, either deliberately set or accidental (NASA FIRMS, 2018). While fires are often perceived as hazards, in specific ecosystems, they serve a crucial role in maintaining balance. For instance, certain plant species rely on high-temperature conditions created by fires for seed release, and fires can clear undergrowth and brush, aiding forest health. Human activities, like slash-and-burn agriculture, also utilize fire to clear fields, remove crop remnants, enrich the soil, and create pasture areas. The VIIRS Fire and Thermal Anomalies layer is a valuable tool for studying the spatial and temporal patterns of fires, identifying persistent hot spots like volcanoes and gas flares, and pinpointing sources of air pollution from smoke, with potential health impacts. In comparison, the 375m I-band data complements MODIS fire detections by offering similar hotspot identification capabilities. However, its enhanced spatial resolution of

375 meters provides a more detailed response to relatively small fires and offers improved mapping of larger fire perimeters (Figure 2.6). Furthermore, it demonstrates superior nighttime performance. As a result, these data are well-suited for applications related to fire management, such as near real-time alert systems, and various scientific research endeavors requiring precise fire mapping (Schroeder & Giglio, 2018).

Figure 2.6 : The VIIRS (Visible Infrared Imaging Radiometer Suite) Fire and Thermal Anomalies (Day, 375m) Imagery on 28.07.2023

2.6.1.3 Sentinel-5P OFFL AER AI: Offline UV Aerosol Index

The Ultraviolet Aerosol Index (UVAI) is the metric used to quantify aerosol levels as detected by TROPOMI. The UVAI is determined through a relatively straightforward calculation that takes into account variations in Rayleigh scattering across different ultraviolet wavelengths, particularly in regions where ozone absorption is minimal. This calculation can even be performed in the presence of cloud cover, allowing for daily, worldwide coverage. A positive AAI value signifies the existence of aerosols that absorb ultraviolet (UV) light, such as dust and smoke (Figure 2.7). This capability proves invaluable for monitoring the progression of sporadic aerosol phenomena stemming from events such as dust storms, volcanic eruptions, and biomass burning (ESA, 2021).

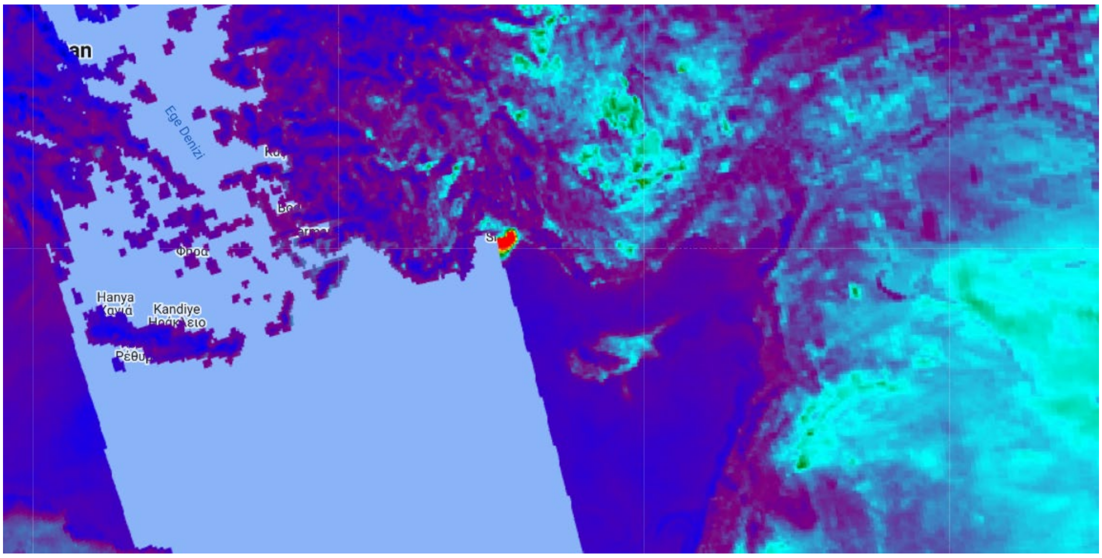

Figure 2.7 : Sentinel-5P OFFL AER AI: Offline UV Aerosol Index Imagery on 28.07.2023

2.7 Methods

2.1.6 The Weather Research and Forecasting with Chemistry (WRF-CHEM)

The 'online' WRF/Chem model is a fully integrated system that has been developed, ensuring seamless synergy between its air quality and meteorological components. These components share the same transport scheme, grid structure, physics schemes, and operate with synchronized time steps (Figure 2.8). The chemistry module incorporates features such as dry deposition, biogenic emissions, chemical mechanisms, advanced photolysis schemes, and a state-of-the-art aerosol module (Grell et al., 2005). This integration enhances the precision of air quality forecasts and deepens our comprehension of the dynamic interplay between atmospheric chemistry and meteorological conditions. WRF-Chem represents an integration of both chemical and dynamic processes at each time step, a critical feature that not only facilitates the exploration of interactions between aerosols, weather, and climate but also significantly benefits air quality research (Baklanov et al., 2014). This versatile model serves multiple purposes, encompassing dispersion forecasts, such as those related to volcanic ash, dust, smoke, or other potentially hazardous substances. Additionally, WRF-Chem is instrumental in the prediction and investigation of air quality, accounting for interactions involving aerosol-radiation and aerosol-microphysics. Moreover, it enables the comprehensive examination of intricate relationships among chemistry, aerosols, and various atmospheric phenomena (Powers et al., 2017).

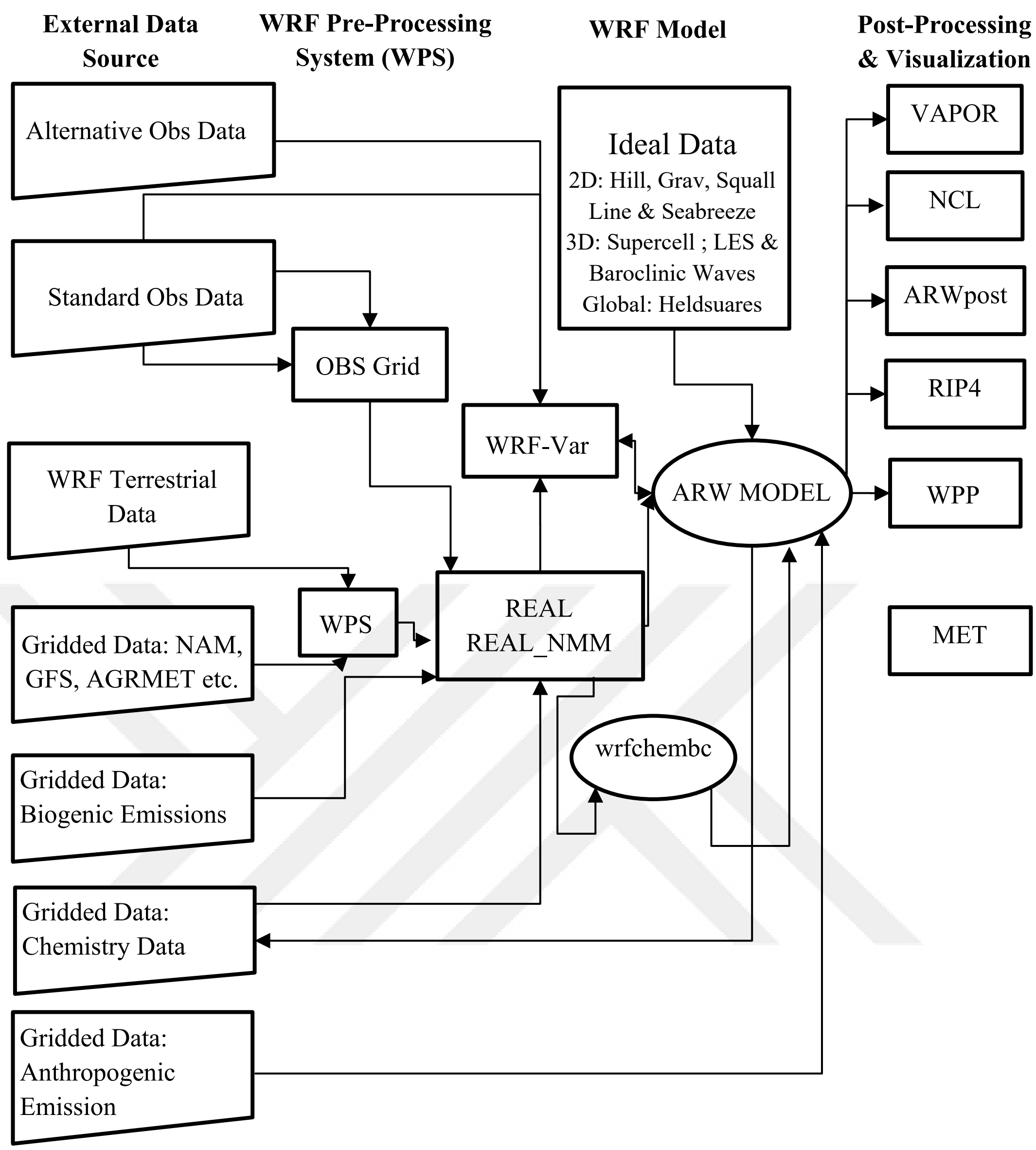

Figure 2.8 : Diagram of WRF-Chem processes

2.7.1.1 The Weather Research and Forecasting Pre-Processing System (WPS)

The Weather Research and Forecasting with Chemistry (WRF-Chem) model relies on the WRF Pre-Processing System (WPS) to prepare input data and grids for its simulations. The WPS is a collection of tools and programs designed to streamline the initial setup of WRF and its various configurations, including WRF-Chem. WPS comprises three key parts:

- Geogrid: This component creates a WRF domain by interpolating data from global datasets onto a local domain. It sets up the computational grid and defines its geographical extent.

- Ungrib: The ungrib utility extracts meteorological fields from external datasets (e.g., GRIB files) that WRF needs as initial and boundary conditions.
- Metgrid: Metgrid interpolates the meteorological fields from ungrib onto the model grid, creating the necessary input files for the WRF model.

2.7.1.2 Gridded Chemistry Data Input to WRF-CHEM

The integration of chemical processes into the Weather Research and Forecasting with Chemistry (WRF-CHEM) model necessitates the provision of supplementary data pertinent to atmospheric chemistry.

- Emissions Data: This includes information on the emission sources of chemical species, such as pollutants, aerosols, and greenhouse gases. Emissions data can come from various sources, including inventories and measurements.
- Chemical Boundary Conditions: WRF-CHEM requires boundary conditions for chemical species at the model's outer boundaries, often obtained from global or regional chemistry models or observational data.
- Chemical Mechanism: It must specified a chemical mechanism, which describes the chemical reactions and species interactions to be simulated in the model. Common mechanisms include CBM-Z, MOZART, and RADM2.

When using WRF-CHEM, additional data related to atmospheric chemistry, including emissions data, chemical boundary conditions, chemical mechanisms, and initial conditions, must be provided alongside the meteorological data prepared by WPS. WPS helps in setting up the model's computational domain and grid, which is essential for both WRF and WRF-CHEM simulations.

2.1.7 Configuration options of WRF-CHEM Model

In this thesis, we utilized the Weather Research and Forecasting with Chemistry (WRF-CHEM) model to investigate the dynamics of the Antalya Manavgat forest fire event and its impact on air quality. Table 2.3 outlines the comprehensive configuration options employed in the WRF-CHEM model, providing detailed insight into the setup utilized for our simulations. Our model consisted of two domains, covering a spatial extent of 40x30 and 61x46 grid points in the east-west and south-north directions, respectively. With 50 vertical levels, a timestep of 15 seconds, and a resolution of 9x9 km for the outer domain and 3x3 km for the inner domain, our model could capture the intricate atmospheric processes at both regional and local scales. The atmospheric processes in the model were based on data from the ECMWF ERA5 Reanalysis for meteorological boundaries, with additional input from SST for auxiliary meteorological boundaries. Cloud microphysics were simulated using the WSM6 scheme, while the boundary layer was parameterized using the MYJ scheme, and cumulus clouds were represented using the Grell-3 scheme. Radiation processes, including longwave and shortwave radiation, were modeled using the RRTMG scheme. The land surface was described using the Noah-MP scheme, and the surface layer was parameterized using the Eta Similarity scheme. Importantly, the chemistry process in our simulations was governed by the GOCART scheme coupled with RACM-KPP, enabling the accurate representation of chemical reactions and aerosol formation processes associated with the forest fire emissions. Overall, this comprehensive configuration of the WRF-CHEM model allowed us to effectively simulate the complex interactions between meteorology and chemistry and assess their implications for air quality during the forest fire event.

Table 2.3 : Configuration options of WRF-CHEM Model.

General Options	
Number of Domain	2
East-West	40, 61
South-North	30, 46
Vertical Levels	50
Timestep	15
Resolution	9×9 km, 3×3km
Atmospheric Process	
Meteorological Boundary	ECMWF ERA5 Reanalysis (Hersbach et al., 2023)
Meteorological Boundary Auxinput4	ECMWF ERA5 Reanalysis SST (Hersbach et al., 2023)
Cloud microphysics	WSM6 (Hong and Lim, 2006)
Boundary layer	MYJ (Janjić, 1994)
Cumulus clouds	Grell-3 (Grell and Dévényi, 2002)
Longwave radiation	RRTMG (Iacono et., 2008)
Shortwave radiation	RRTMG (Iacono et., 2008)
Land surface	Noah-MP (He et al., 2023)
Surface layer	Eta Similarity (Janjic, 2002)
Chemistry Process	
Chemistry scheme	GOCART coupled with RACM-KPP

3. RESULTS

3.1 Synoptic Analysis of Manavgat Forest Fire

The development, escalation, and mitigation of forest fires are intricately linked to atmospheric dynamics and meteorological parameters. Various factors such as high temperatures, low relative humidity within the atmospheric boundary layer (ABL), absence of precipitation, strong winds, and prevailing wind directions play pivotal roles and warrant meticulous examination (Romanov et al., 2022). In the context of the forest fires that ravaged the Manavgat district of Antalya between July 26 and August 9, 2021, atmospheric conditions emerged as primary determinants shaping the fires' duration, intensity, trajectory, and impact. Synoptic composite charts spanning from surface levels to upper atmospheric levels (e.g., 1000, 850, 700, 500, 300 hPa) were utilized during this period to delineate the prevailing meso- or synoptic-scale structures (Figure 3.1).

Examining the 1000 hPa chart, a notable observation was the influence of the Basra Low-Pressure Center (BLPC), a recurring feature that significantly impacts Turkey, particularly during the summer months. This BLPC, characterized by its thermal origin and continental warm-core pressure center nature, exerts considerable influence over the central and southern latitudes of Turkey. Owing to its thermal origin, the BLPC sustains dominance over its affected regions for extended durations. During the specified period, this deep BLPC situated in the southeast of Turkey facilitated the transport of dry and warm air into the country via easterly flows. Notably, the Manavgat district experienced the northeasterly flows associated with this deep BLPC (refer to Fig. 12.B).

At the 850 hPa level, a low-pressure center was observed almost directly above the BLPC within the vertical atmosphere. This center persisted in channeling dry and warm air towards the Manavgat district through northeasterly flows at an altitude of approximately 1500m above sea level. Analysis of relative humidity values at this level revealed consistently low readings, hovering around 30% throughout Antalya.

Such conditions underscored the dryness of the atmosphere, exacerbating the susceptibility to fire outbreaks and facilitating rapid fire spread upon ignition.

Continuing the meteorological analysis, at the 700 hPa level, approximately 3000m above sea level, similar trends of dry and warm air prevailed. This atmospheric layer often serves as a critical threshold for convective activities, which, if triggered, could yield short-lived yet intense local rainfall—a potential boon for fire containment efforts. However, during this period, such convective events appeared limited, further compounding the challenges faced in controlling the wildfires. Similarly, at the 500 hPa and 300 hPa levels, upper-level flows were northwesterly and westerly, respectively.

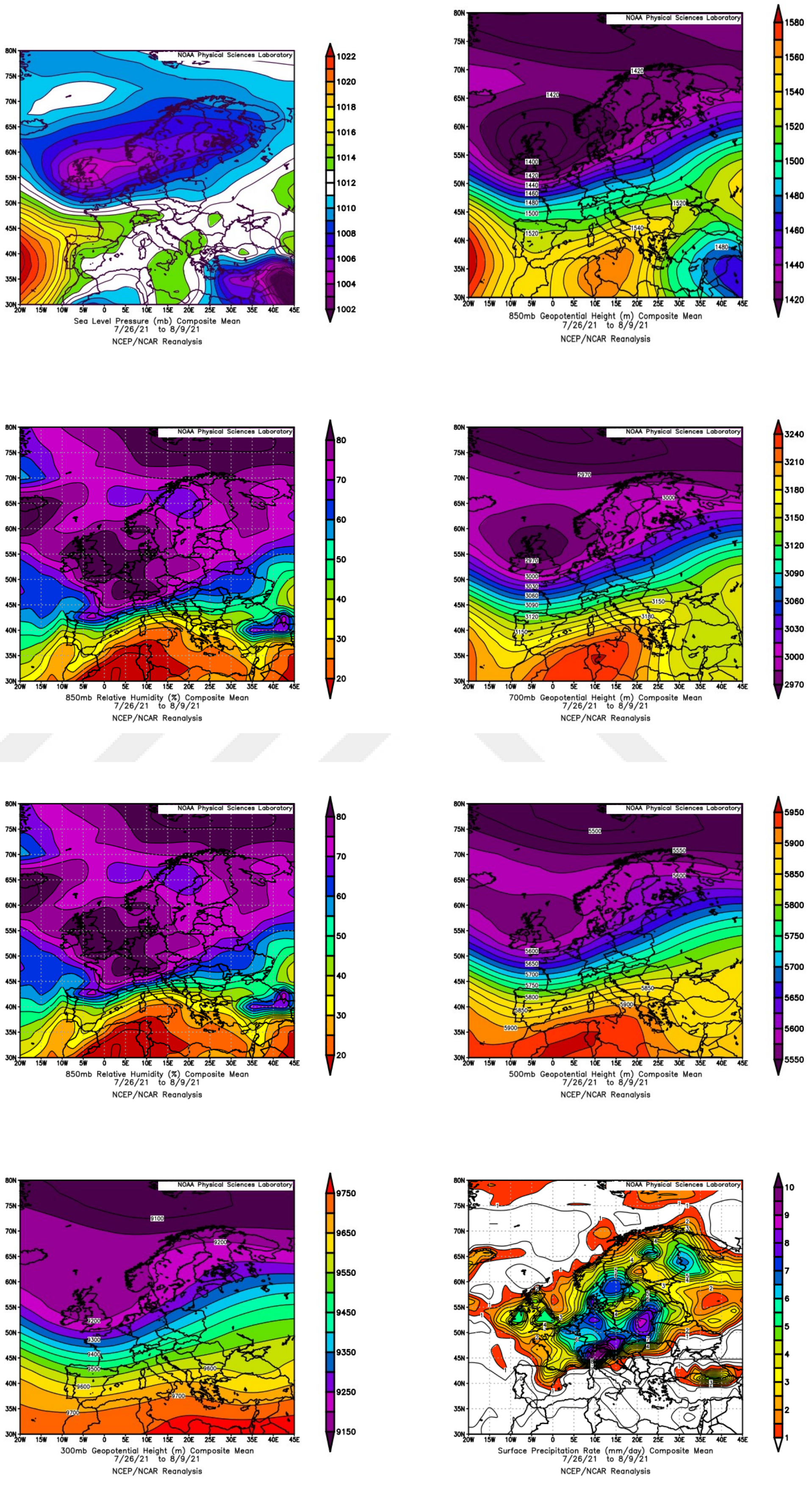

Figure 3.1 : Synoptic composite charts during fire event.

3.2 Micrometeorologic Analysis of Manavgat Forest Fire

Understanding the intricate interplay between large-scale atmospheric conditions and localized surface-level meteorological phenomena is paramount in comprehending the dynamics of forest fires. The provided images (Figure 3.2) vividly depict the manifestation of the Foehn effect on the lee side of the Toros Mountains, coinciding with the onset of a forest fire on February 28, 2021, and February 29, 2021. On the left, the three-dimensional wind trajectory from the WRF-Chem model illustrates the movement of air masses over the mountain range, with varying line patterns denoting wind trajectories at different altitudes. This model serves as a crucial tool in elucidating the development of the Foehn effect by showcasing airflow patterns over the mountains, ultimately resulting in the warming and drying of air as it descends on the leeward side—a phenomenon known to exacerbate conditions conducive to wildfires. On the right side of the image, a surface weather chart provides further insight. Isobars delineate atmospheric pressure, while the color gradient signifies temperature fluctuations, and arrowed barbs depict wind direction and velocity. Notably, the chart accentuates the lee side of the Toros Mountains, distinctly highlighting this region with temperatures around 40°C, underscoring the profound impact of local topography on micrometeorological conditions. At 9:00 UTC (12:00 LST - UTC+3) on the pivotal initial day, coinciding with the forest fire's onset, the WRF model projected a temperature of 40.15°C and a relative humidity of 15.58%. Concurrently, observed measurements recorded a temperature of 39.7°C with a relative humidity of 10%. Throughout the first two days, the WRF model depicted temperatures ranging from 27.22°C to 40.15°C, with relative humidity values fluctuating between 15.58% and 42.47%. Corresponding observational data revealed temperatures spanning from 33.5°C to 40.8°C, with relative humidity levels varying from 8% to 23%. This alignment between WRF data and observations underscores the agreement on conditions conducive to rapid wildfire development and spread. Particularly noteworthy is the consistency in relative humidity, as reflected in observed data, which aligns with the expected drying effect of Foehn winds on the leeward side of the Toros Mountains during the initial two days. This drying effect significantly contributes to the exacerbation of forest fire conditions. However, in the subsequent two days, both the model and observations indicate a notable shift in meteorological conditions. Relative humidity levels surged to around 80%, while temperatures concurrently decreased to 27-28°C. This significant alteration in conditions heralds a relatively humid and cooler atmosphere, marking a distinct departure from the preceding days' patterns. Such shifts in weather dynamics can have profound implications for fire behavior and management strategies, necessitating a nuanced understanding of evolving meteorological conditions to effectively mitigate wildfire risks.

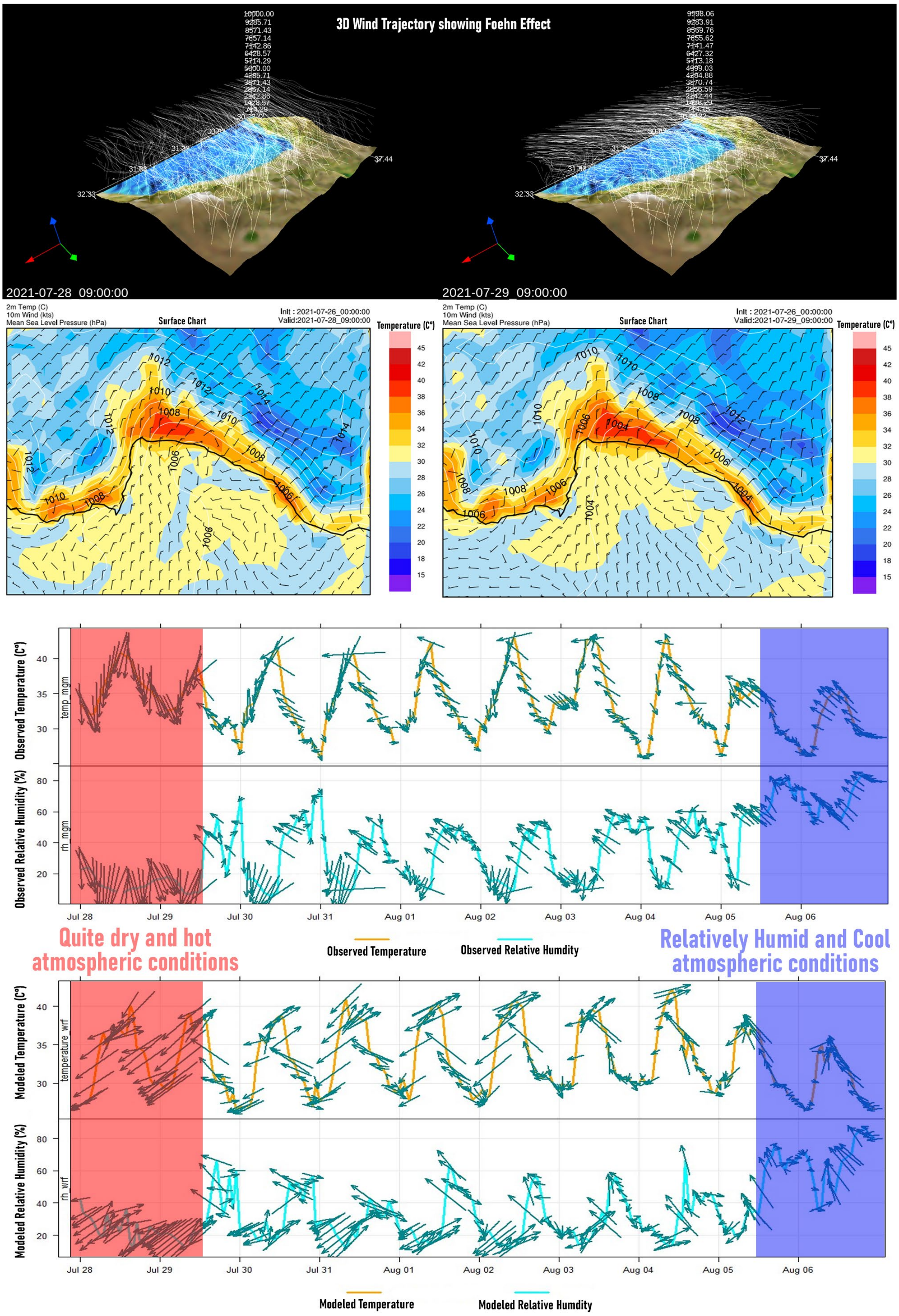

Figure 3.2 : 3D Wind trajectory visualization over the Toros Mountains indicating Foehn wind patterns (above) surface weather chart (middle), time-series of observed and WRF-Chem meteorological variables (below).

3.3 Geospatial Analysis of the Event

To comprehensively understand the spread and impact of the Antalya Manavgat forest fire in 2021, geospatial analyses necessitated specific dates. Thus, analyses were conducted utilizing outputs from the WRF-Chem model alongside various satellite images.

As illustrated in Figure 3.3 and summarized in Table 3.1, the Antalya Manavgat forest fire in 2021 ignited on July 28, rapidly escalating into a major disaster. The situation exacerbated on July 29, witnessing an intensification and swift spread of the fire. By August 2, the fire had reached its peak geographical extent, presenting formidable challenges to firefighting endeavors. However, concerted efforts saw significant progress, and by August 6, the fire was successfully contained and extinguished. This chronological delineation of events underscores the temporal evolution and severity of the forest fire, highlighting the critical phases from ignition to containment. Incorporating both model outputs and satellite data, provide invaluable insights into the spatiotemporal dynamics of wildfire incidents.

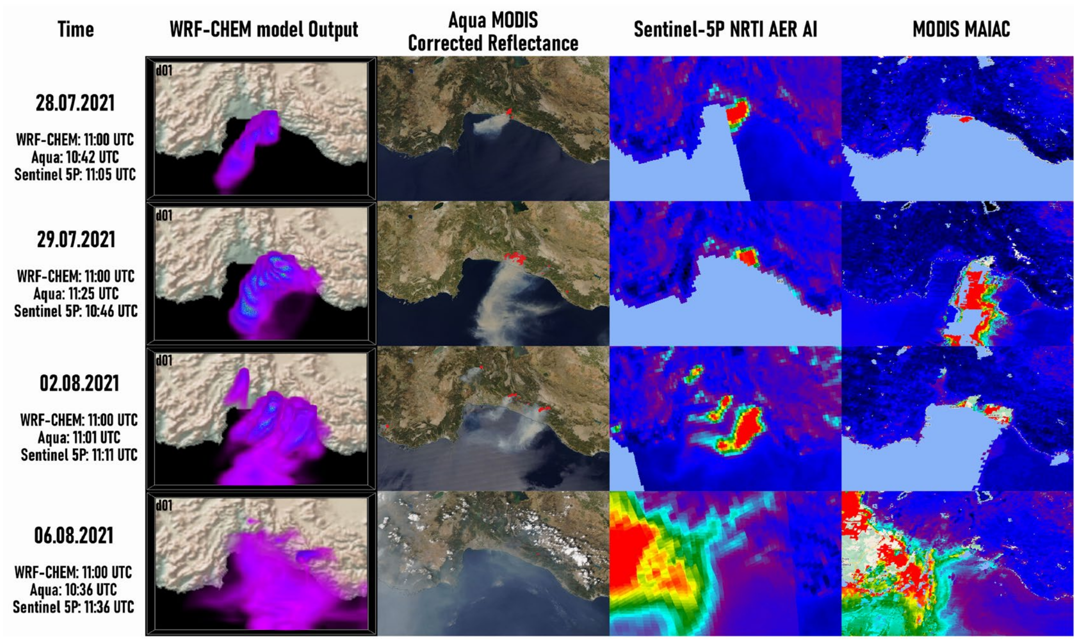

Figure 3.3 : Visualization of both model and satellite observations on important dates of Antalya Manavgat forest fire disaster.

Table 3.1 : Important dates of Antalya Manavgat forest fire disaster.

Date	Event
28.07.2021	Onset of the Manavgat Wildfire
29.07.2021	Peak Levels of Aerosol Optical Depth (AOD) and PM_{10} Particulates Detected in ground station
02.08.2021	Maximum Geographical Spread of the Wildfire
06.08.2021	Successful Containment and Extinguishment of the Wildfire

3.4 Hotspot Detection

Figure 3.4 presents a comparative visualization portraying modeled data on the left, derived from the WRF-Chem model, and actual satellite detection of thermal anomalies linked to fire hotspots on the right, obtained from the VIIRS. This comparison spans four distinct dates during the Antalya Manavgat forest fire incident in 2021. The alignment between hotspots predicted by the WRF-Chem model and those detected by VIIRS satellite observations is striking. This consistency implies a robust predictive capability of the WRF-Chem model for this specific event. The congruence between modeled and observed hotspots underscores the model's effectiveness in capturing and forecasting the spatial distribution of fire activity. Such a comparative analysis not only validates the reliability of the WRF-Chem model but also enhances our understanding of its utility in real-time monitoring and predictive modeling of wildfire events.

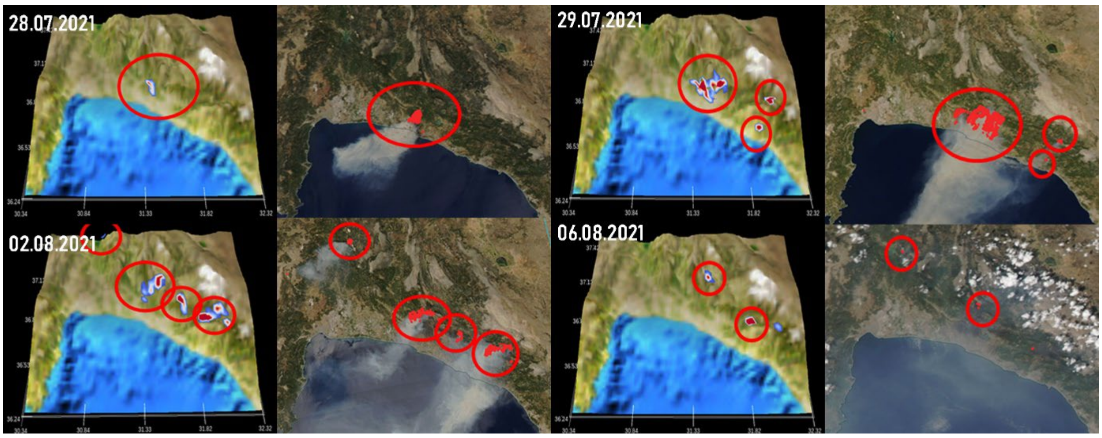

Figure 3.4 : Comparative Analysis of Forest Fire Hotspots: WRF-Chem (Left) vs. VIIRS (Right).

3.5 Performance of WRF-CHEM for Meteorological Variables

The correlation coefficient analysis for various meteorological parameters reveals robust patterns across the observed locations (Figure 3.5). Temperature exhibits uniformly strong positive relationships, with Kepez leading with a coefficient of 0.94, closely followed by Muratpasa (0.84), Kumluca (0.91), Manavgat (0.84), Alanya (0.82), Serik (0.58), and Gazipasa (0.62). These high coefficients indicate a consistent agreement between temperature measurements or model outputs and reference data across these regions. Similarly, relative humidity measurements or model outputs demonstrate solid positive correlations across most stations. Alanya (0.80) and Manavgat (0.80) exhibit the strongest correlations, trailed closely by Muratpasa (0.74), Gazipasa (0.64), Kumluca (0.68), Kepez (0.55), and Serik (0.38), indicating reliable capture of humidity variations in these areas.

The correlations for wind speed exhibit more variability. Muratpasa shows a strong positive correlation (0.61), followed by Manavgat (0.62), Kumluca (0.49), Gazipasa (0.48), Alanya (0.40), Kepez (0.33), and Serik with a notably lower correlation (0.06), highlighting a potential area for improvement in wind speed prediction or measurement at certain locations. Conversely, atmospheric pressure correlation coefficients are consistently high across all reported locations, indicating excellent agreement with the reference data. Muratpasa demonstrates exceptional correlation (0.95), with Gazipasa also exhibiting a very high correlation (0.95), closely followed by Manavgat (0.94), and Serik (0.51). This suggests that pressure data from these locations aligns very well with the reference dataset. Notably, Muratpasa and Manavgat emerge as standout locations with high correlations across all parameters, indicating a strong agreement between model outputs or measurements for these specific sites.

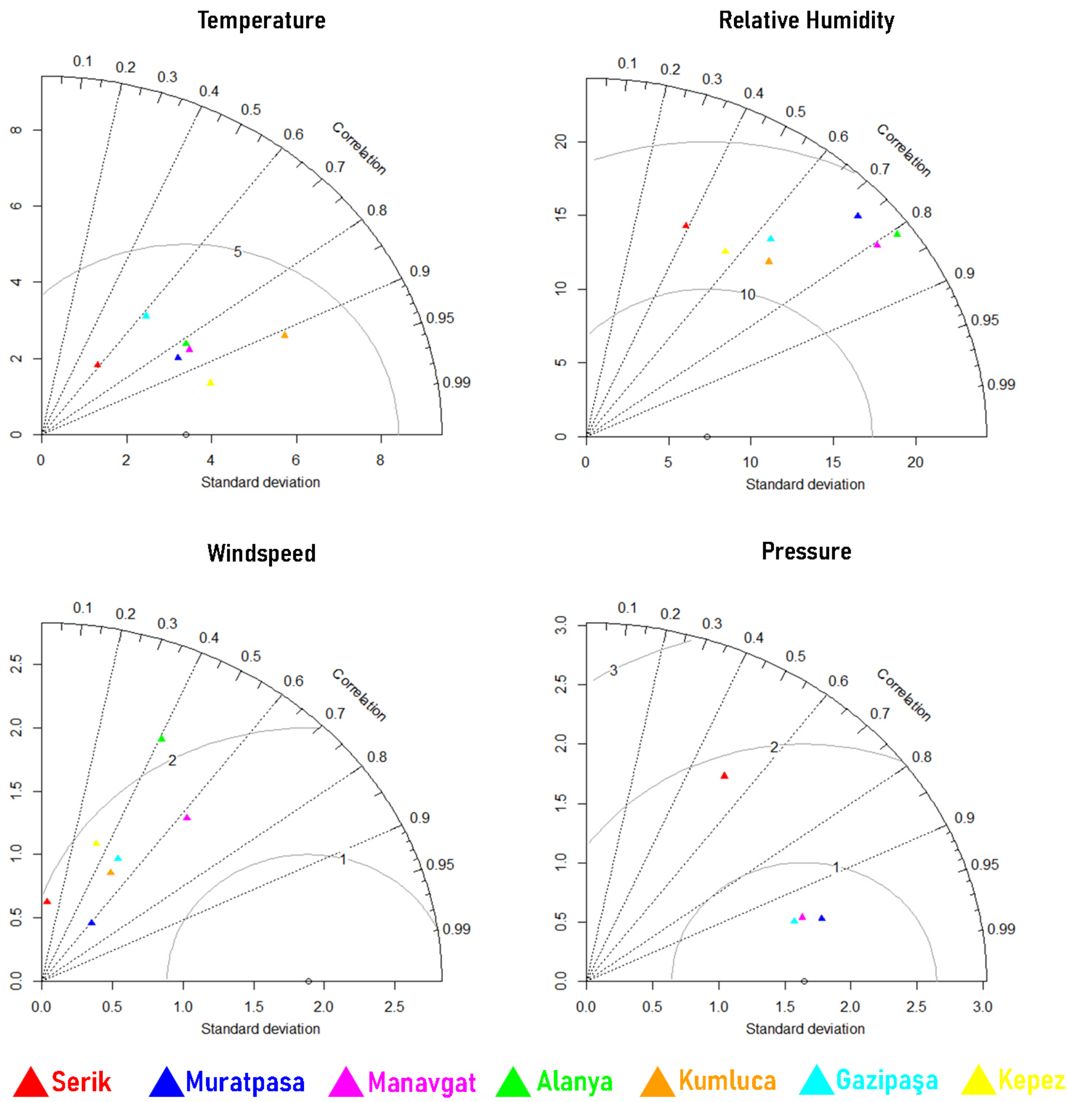

Figure 3.5 : Taylor diagrams of meteorological variables.

3.6 Descriptive Statistics of Measured and Modeled Air Pollutants

In Muratpaşa, both observed and chemically measured PM_{10} levels are available, with the observed PM_{10} mean recorded at 40.0 µg/m³ and the chemical measurement slightly lower at 37.6 µg/m³ (Table 3.2). The standard deviation for observed PM_{10} levels is 13.7 µg/m³, indicating a moderate degree of variability around the mean, while the chemical measurements exhibit a slightly lower standard deviation of 12.6 µg/m³.

Moving to Serik, observed PM_{10} levels have a mean of 34.6 µg/m³, with a standard deviation of 13.9 µg/m³, while chemically measured levels show a slightly higher mean of 38.1 µg/m³ and a standard deviation of 12.4 µg/m³ (Figure 3.6).

However, in Manavgat, there's a notable similarity between observed and chemical measurements. The observed PM_{10} levels exhibit a significantly higher mean of 87.0 µg/m³, with a substantial standard deviation of 94.0 µg/m³, indicating a considerable variability in the data. On the other hand, the chemically measured PM_{10} levels show a lower mean of 73.1 µg/m³ and a standard deviation of 81.9 µg/m³, still indicating notable variability but to a lesser extent than the observed data.

In Alanya, both observed and chemical PM_{10} levels are relatively lower compared to other locations, with observed PM_{10} levels showing a mean of 21.4 µg/m³ and a standard deviation of 4.7 µg/m³, while chemically measured levels have a slightly higher mean of 25.1 µg/m³ and a standard deviation of 7.9 µg/m³.

A kurtosis near 0, as seen in Alanya_CHEM (0.0) and Muratpasa_CHEM (-0.7), indicates a distribution that closely resembles a normal distribution in terms of its tails. Positive kurtosis values, like those in Serik_CHEM (0.3), Muratpasa_obs (0.1), and Alanya_obs (7.6), indicate distributions with heavier tails than a normal distribution, which may be prone to more extreme values. The very high kurtosis values observed in Manavgat_obs (47.4) and Manavgat_CHEM (27.7) suggest exceptionally heavy tails, indicating a high likelihood of extreme values far from the mean, which significantly differs from the normal distribution (Figure 3.7).

Table 3.2 : Descriptive Statistics of observed and modeled PM_{10}

PM_{10} (µg/m³)	mean	sd	median	min	max	range	skew	kurtosis
Muratpasa_obs	40.0	13.7	37.7	17.4	83.1	65.7	0.7	0.1
Muratpasa_CHEM	37.6	12.6	35.9	21.5	70.4	48.8	0.5	-0.7
Serik_obs	34.6	13.9	31.2	11.5	73.7	62.2	0.7	-0.2
Serik_CHEM	38.1	12.4	35.5	20.4	80.0	59.6	0.9	0.3
Manavgat_obs	87.0	94.0	61.6	35.7	966.6	930.9	6.3	47.4
Manavgat_CHEM	73.1	81.9	47.6	20.4	750.5	730.2	4.6	27.7
Alanya_obs	21.4	4.7	20.9	8.7	52.1	43.3	1.5	7.6
Alanya_CHEM	25.1	7.9	24.6	7.4	46.8	39.4	0.5	0.0

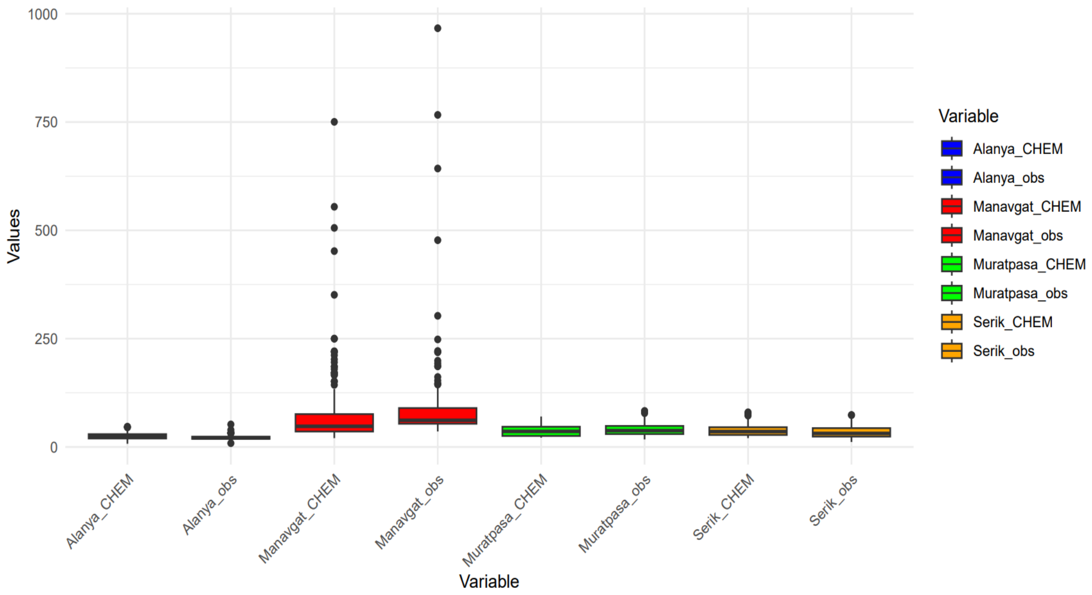

Figure 3.6 : Boxplot of observed and modeled PM_{10}

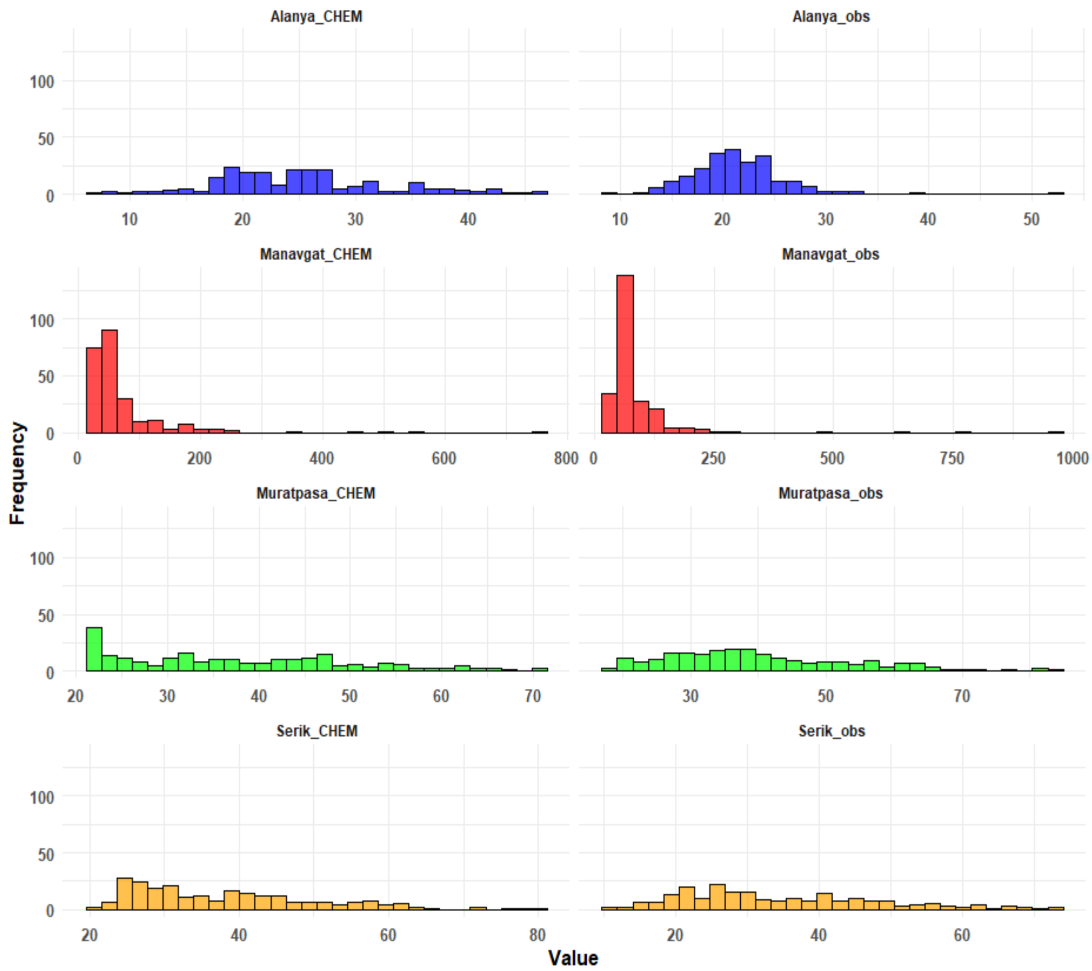

Figure 3.7 : Histogram of observed and modeled PM_{10}

3.7 Pollution Calendars and Air Quality Index (AQI)

EPA The Air Quality Index (AQI) measures the concentration of pollutants in the air, specifically focusing on particulate matter with a diameter of 10 micrometers or less (PM_{10}). The AQI categorizes air quality based on the 24-hour mean concentration of PM_{10}. In the range of 0-54 µg/m³, air quality is deemed good; between 55-154 µg/m³, it's considered moderate. When levels rise to 155-254 µg/m³, individuals with sensitivity to pollution may experience discomfort. At 255-354 µg/m³, the air becomes unhealthy, and as it exceeds 355 µg/m³, it progresses to bad, hazardous, and potentially hazardous conditions (Table 3.3).

Table 3.3 : Air Quality Index (AQI) Categories Based on 24-Hour Mean PM_{10} Concentration

AQI	PM_{10} (µg/m3) 24h mean	Condition
0-50	0-54	Good
51-100	55-154	Moderate
101-150	155-254	Sensitive
151-200	255-354	Unhealty
201-300	355-424	Bad
301-400	425-504	Hazardous
401-500	505-604	Hazardous

At the Muratpaşa station, it exhibits a good AQI before August 5th to 6th and maintains an average AQI during these dates (Figure 3.8). Meanwhile, at the Serik station, the AQI remains consistently good throughout the monitoring period. However, in the Manavgat station, although the air quality starts off good at the beginning of the forest fire incident, it deteriorates the following day (the most severe day of the incident) to a sensitive level. Subsequently, the air quality undergoes a gradual improvement, eventually reaching an average AQI. Conversely, at the Alanya station, the air quality consistently remains at a good AQI level throughout the entire period of observation.

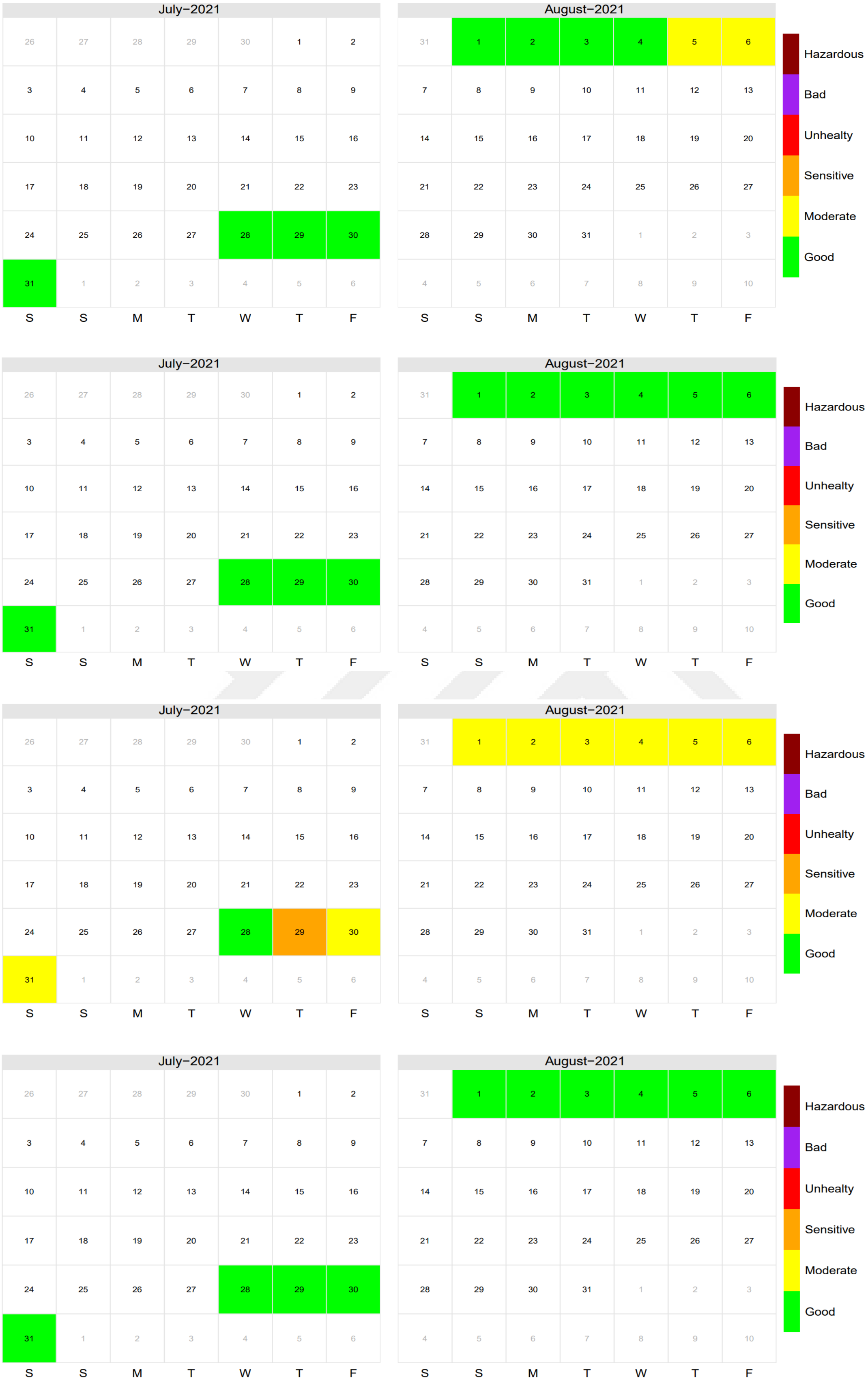

Figure 3.8 : Pollution calendars of Muratpaşa, Serik, Manavgat, and Alanya stations, respectively, colorized according to EPA AQI classification.

3.8 Performance of WRF-CHEM for AOD and PM_{10}

Figure 3.9 presents a three-panel comparison, offering a comprehensive view of Aerosol Optical Depth (AOD) data from three distinct sources: the WRF-Chem model, MODIS MAIAC satellite observations, and Sentinel-5P satellite observations. Each row corresponds to the same day, facilitating a nuanced day-to-day and source-to-source comparison of AOD, a key indicator of aerosol presence and density in the atmosphere. This parameter is commonly utilized to monitor pollution or, in the context of this thesis, to track smoke dispersion from wildfires. On July 28, both the model and MODIS data depict moderate AOD values, while Sentinel-5P data indicates higher Aerosol Absorption Index (AAI). July 29 witnesses a substantial escalation in AOD and AAI across all three sources, signifying a significant influx of aerosols into the atmosphere due to the intensification of the forest fire. By August 2, the distribution of aerosols undergoes a shift. The WRF-Chem model and MODIS data reveal multiple regions with elevated AOD, whereas Sentinel data suggests extensive aerosol absorption. Come August 6, AOD values exhibit a decline in the model and MODIS data, while Sentinel data still indicates heightened aerosol levels, indicative of a potential aerosol transportation event. The consistent elevation of AOD values across all three sources on July 29 and August 2 corroborates the severity of the forest fire during those periods. The gradual reduction in AOD values by August 6 suggests a mitigation in fire activity.

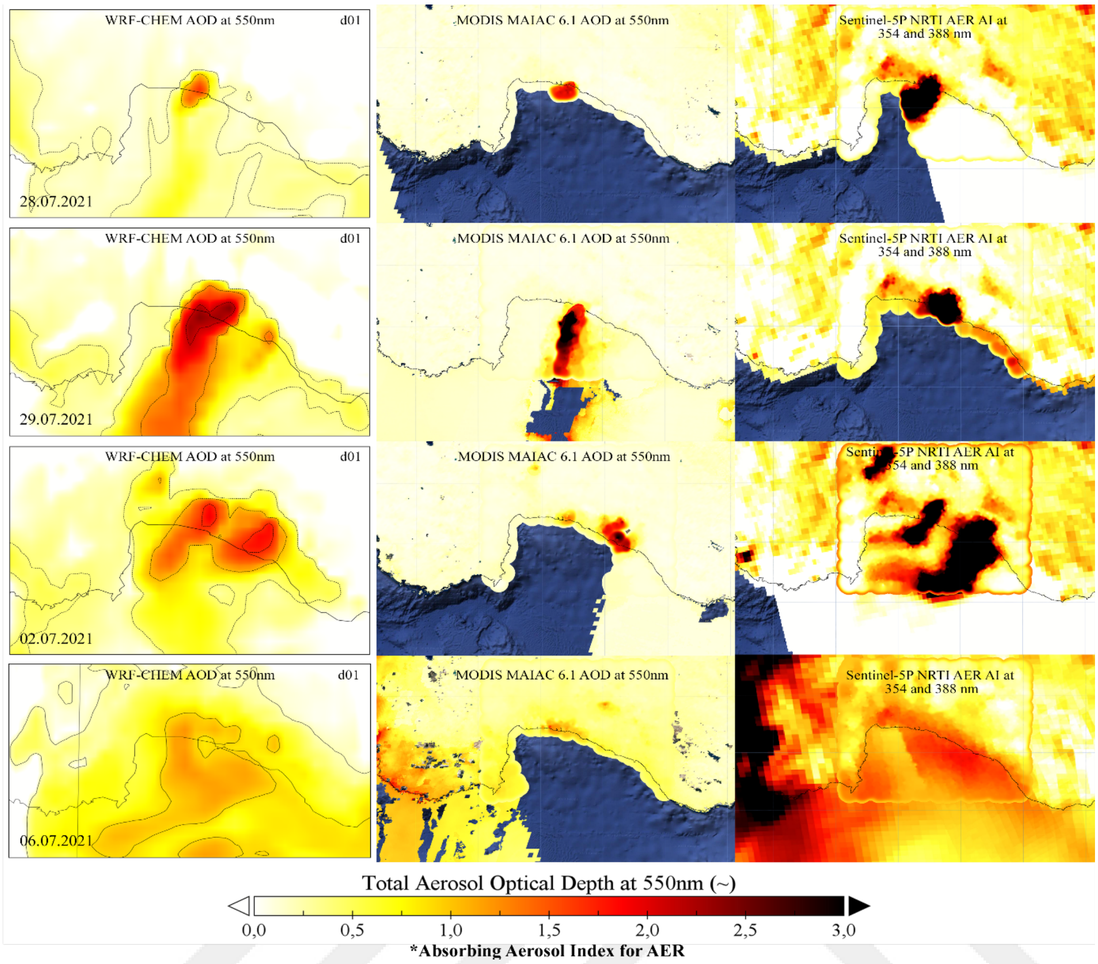

Figure 3.9 : Spatial Distribution of AOD and AAI from WRF-CHEM, MAIAC, NRTI AER AI.

In Table 3.4, observations from the Muratpaşa Station grid on July 28, 2021, reveal a WRF-Chem AOD of 0.24, closely aligned with the MAIAC AOD of 0.249, indicating a high level of agreement between modeled and satellite-derived AOD values. Additionally, the AER AAI is reported at 0.99, further supporting the concordance between model and satellite aerosol measurements. By August 6, the WRF-Chem AOD reaches its zenith at 0.72, closely mirroring the MAIAC AOD of 0.72. This close correspondence suggests that the model aptly captured the peak of the aerosol event as evidenced by satellite observations. However, there remains a notable disparity in the AER AAI value, which records at 1.51. While the WRF-Chem model aligns well with MAIAC data, this discrepancy underscores potential differences in how aerosol properties are characterized between the model and AER AAI observations.

The data from the Serik Station on August 1 reveals a notable surge in Aerosol Optical Depth (AOD) values compared to the previous day. The WRF-Chem model reports an AOD of 0.36, marking a considerable decrease from the MAIAC AOD of 1.36 and the

AER AAI of 1.29. This discrepancy suggests that the WRF-Chem model may not have effectively captured aerosol transportation on this particular day, as indicated by satellite observations. Conversely, on August 6 at the Serik Station, AOD values recorded a significant increase. MAIAC reports an AOD of 0.92, while AER AAI records 1.46, both substantially higher than the WRF-Chem AOD of 1.25. This notable rise is consistent with the trend observed at the Muratpaşa Station, underscoring the widespread aerosol event during this period.

At the Manavgat Station grid, on July 29, the WRF-Chem model registered a notable Aerosol Optical Depth (AOD) of 2.05, indicative of a substantial presence of aerosols in the atmosphere. This observation aligns closely with the MAIAC AOD, which recorded a similarly high value of 2.12, underscoring the dense concentration of aerosols attributed to the forest fire. Additionally, the AER AAI reported a high value of 4.856, further reinforcing the evidence of significant aerosol presence on this day. The following day, July 30, saw a spike in WRF-Chem AOD to 1.78, closely mirroring the AER AAI of 3.97, while the MAIAC AOD measured 1.89. This increase in AOD values suggests a continued presence of aerosols in the atmosphere, consistent with the observations from the previous day.

At the Alanya Station grid, on July 29, the WRF-Chem model indicates an Aerosol Optical Depth (AOD) of 1.12, significantly higher than the MAIAC AOD of 0.17. Concurrently, the AER AAI records at 0.37. However, on August 4, AOD values exhibit a notable shift. MAIAC reports AOD values of 0.41, while AER AAI measures at 0.055, and WRF-Chem records 0.31. This discrepancy between MAIAC and AER AAI values is notable, with MAIAC indicating a moderate AOD while AER AAI suggests lower aerosol absorption. Analysis unveils a variable degree of correlation between AOD data from MAIAC and AAI sources and WRF-Chem model outputs across different monitoring stations. Particularly at the Muratpaşa Station, a strong positive correlation between MAIAC AOD and WRF-Chem AOD data ($r = 0.94$) suggests close alignment of the model with MAIAC satellite observations in this region. Conversely, correlations with AER AAI data are moderate ($r = 0.45$ with WRF-Chem AOD and $r = 0.35$ with MAIAC AOD), indicating some divergence in aerosol property measurements by different sources.

The Serik Station findings unveil notably diminished correlations across various metrics. Notably, the most robust association observed was a moderate correlation between MAIAC AOD and WRF-CHEM AOD, indicating a correlation coefficient of 0.41. These outcomes hint at substantial limitations within the WRF-Chem model's capability to accurately depict aerosol concentrations at the Serik Station. Particularly noteworthy is the discernible impact of meteorological conditions on aerosol transport, notably evident on August 1st.

At the Manavgat Station, significant correlations were evident across various data pairs, with particularly striking positive correlations noted between MAIAC AOD and WRF-Chem AOD (r = 0.93), as well as between AER AAI and WRF-Chem AOD (r = 0.80) (Figure 3.10). These findings highlight a remarkable level of agreement, indicating the model's efficacy in capturing aerosol events within this region. Meanwhile, data from the Alanya Station displayed robust correlations between MAIAC and WRF-Chem AOD (r = 0.80), alongside high correlations with AER AAI AOD (r = 0.71). These outcomes underscore the model's reliability in simulating AOD compared to MAIAC, albeit with some variability when juxtaposed with AER AAI measurements.

Table 3.4 : AOD and AAI time series of four station grids.

Merkez Station grid			
date	MAIAC_AOD	AER AAI	WRF-CHEM_AOD
28.07.2021	0.25	1.00	0.25
29.07.2021	0.22	0.96	0.25
30.07.2021	0.30	0.86	0.25
31.07.2021	0.23	1.37	0.25
1.08.2021	0.24	1.21	0.25
2.08.2021	0.29	1.32	0.29
3.08.2021	0.25	0.85	0.24
4.08.2021	0.50	0.76	0.34
5.08.2021	0.46	2.43	0.42
6.08.2021	0.73	1.51	0.73
Serik Station grid			
28.07.2021	0.26	1.48	0.26
29.07.2021	0.30	1.17	0.25
30.07.2021	0.48	1.46	0.33
31.07.2021	0.31	1.35	0.39
1.08.2021	1.36	1.29	0.37
2.08.2021	0.28	1.17	0.70
3.08.2021	0.40	0.78	0.37
4.08.2021	1.22	1.33	0.74
5.08.2021	0.39	1.48	0.42
6.08.2021	0.93	1.46	1.26
Manavgat Station Grid			
28.07.2021	0.18	2.75	0.63
29.07.2021	2.12	4.86	2.05
30.07.2021	1.90	3.98	1.79
31.07.2021	1.31	4.40	1.54
1.08.2021	0.85	3.16	1.23
2.08.2021	0.57	1.09	1.23
3.08.2021	0.43	0.51	0.82
4.08.2021	0.67	0.09	0.69
5.08.2021	0.40	1.06	0.75
6.08.2021	1.11	1.49	1.11
Alanya Station Grid			
28.07.2021	0.09	0.18	0.18
29.07.2021	0.18	0.38	0.6
30.07.2021	0.34	0.62	1.26
31.07.2021	1.24	4.13	1.51
1.08.2021	0.35	4.11	0.86
2.08.2021	0.82	3.39	1.21
3.08.2021	0.21	0.60	0.30
4.08.2021	0.41	0.06	0.31
5.08.2021	0.12	0.86	0.21
6.08.2021	0.55	1.24	0.75

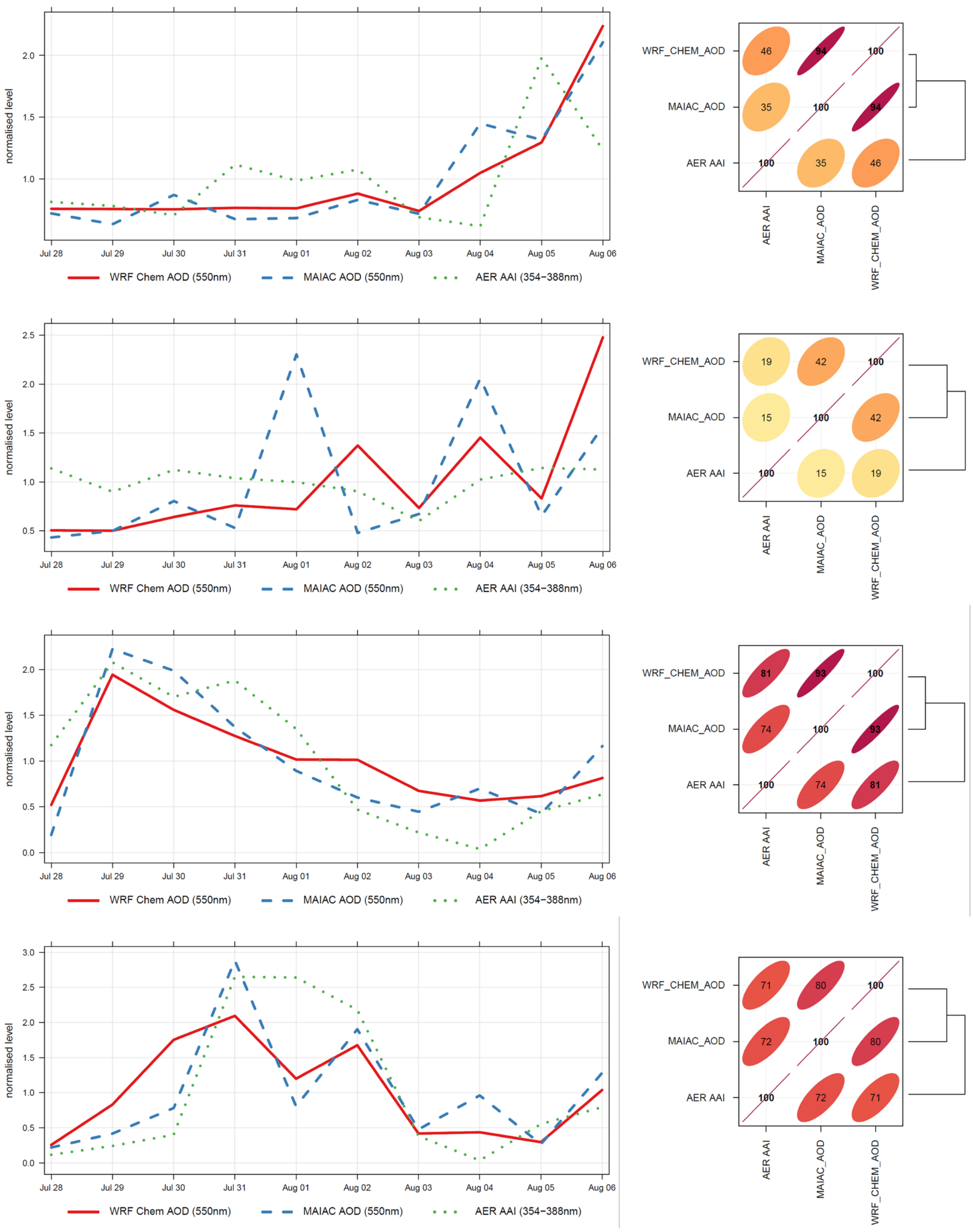

Figure 3.10 : Normalized Time series of AOD and AAI (left) and correlation matrices with dendogram (right).

3.9 Performance of WRF-CHEM PM_{10}

Figure 3.11 provides an in-depth examination of PM_{10} levels across different locations within the Antalya-Manavgat region. Presented as a series of time series plots aligned with Local Standard Time (LST, UTC+3), these visuals juxtapose observed PM_{10} concentrations (obs) with the corresponding predictions generated by the WRF-Chem model. The analysis covers four specific stations: Muratpaşa, Serik, Manavgat, and Alanya.

The performance of the WRF-Chem model at the Muratpaşa station demonstrates a commendable replication of the diurnal variation in PM_{10} levels, reflecting its ability to mirror the typical daily fluctuations inherent in urban settings (Al-Harbi et al., 2019). The time series analysis reveals a close alignment between modeled and observed PM_{10} levels, supported by a strong positive correlation in Muratpaşa (r=0.72). Notably, the model effectively captures a PM_{10} transportation episode observed towards the latter part of the dataset. This indicates the model's proficiency not only in handling regular daily variations but also in simulating sporadic transport phenomena.

The time series analysis of Serik's data unveils a noticeable agreement between observed and modeled PM_{10} levels, albeit with more pronounced variation compared to Muratpaşa. The correlation coefficient for Serik stands at a modest r=0.44, indicating the WRF-Chem model's ability to capture the general trend of PM_{10} fluctuations, albeit with reduced precision in this specific locale. This diminished correlation may stem from the suboptimal performance of the underlying WRF model in accurately representing local meteorological conditions.

The WRF-Chem model demonstrates remarkable performance in Manavgat, notably reflected in its accurate depiction of PM_{10} levels. For instance, on July 29th at 0900 LST (UTC+3), an observed PM_{10} level of 966.5 µg/m³ closely aligns with the model's prediction of 750.5 µg/m³. This close correspondence is further supported by a high correlation coefficient (r=0.82), highlighting the model's precision in replicating real-world conditions, even during extreme pollution events. The simultaneous occurrence of a spike in both observed and modeled data underscores the model's effectiveness in simulating significant pollution events, particularly in the context of the Antalya Manavgat forest fires.

The assessment of ground-level PM_{10} data in Alanya reveals a moderate positive correlation (r=0.50), while AOD measurements exhibit a strong correlation (r=0.80), showcasing a nuanced performance of the WRF-Chem model. The model demonstrates alignment with higher atmospheric aerosol concentrations, as indicated by the AOD data. However, it appears to deviate when estimating ground-level PM_{10}, especially at lower observed values. This divergence suggests that while the model effectively captures aerosol behavior in the atmospheric column represented by AOD measurements, it may not translate this accuracy to the near-surface level where PM_{10} concentrations are measured. This discrepancy underscores the need for further refinement in the model's representation of aerosol dynamics at ground level, potentially through improved parameterization or resolution adjustments. Achieving greater congruence between modeled and observed PM_{10} concentrations would enhance the model's utility in assessing air quality impacts and guiding pollution mitigation strategies in Alanya and similar locations.

The discrepancy observed in the model's performance regarding ground-level PM_{10} predictions versus upper atmosphere AOD data at observation stations necessitates a thorough exploration of atmospheric pollutant dispersion dynamics. To delve deeper into this issue, the subsequent section of the thesis is dedicated to analyzing 3D fire plume modeling, integrating wind trajectories, and scrutinizing PM_{10} cross-sectional data. By employing 3D fire plume modeling, researchers aim to capture the intricate vertical and horizontal movement of pollutants emitted from the fire source. Wind trajectories play a crucial role in this analysis, providing insights into how atmospheric currents disperse pollutants over varying altitudes and distances. Integrating these trajectories with PM_{10} cross-sectional data offers a multi-dimensional perspective on pollutant transport and distribution, aiding in identifying factors contributing to discrepancies between modeled and observed pollutant concentrations.

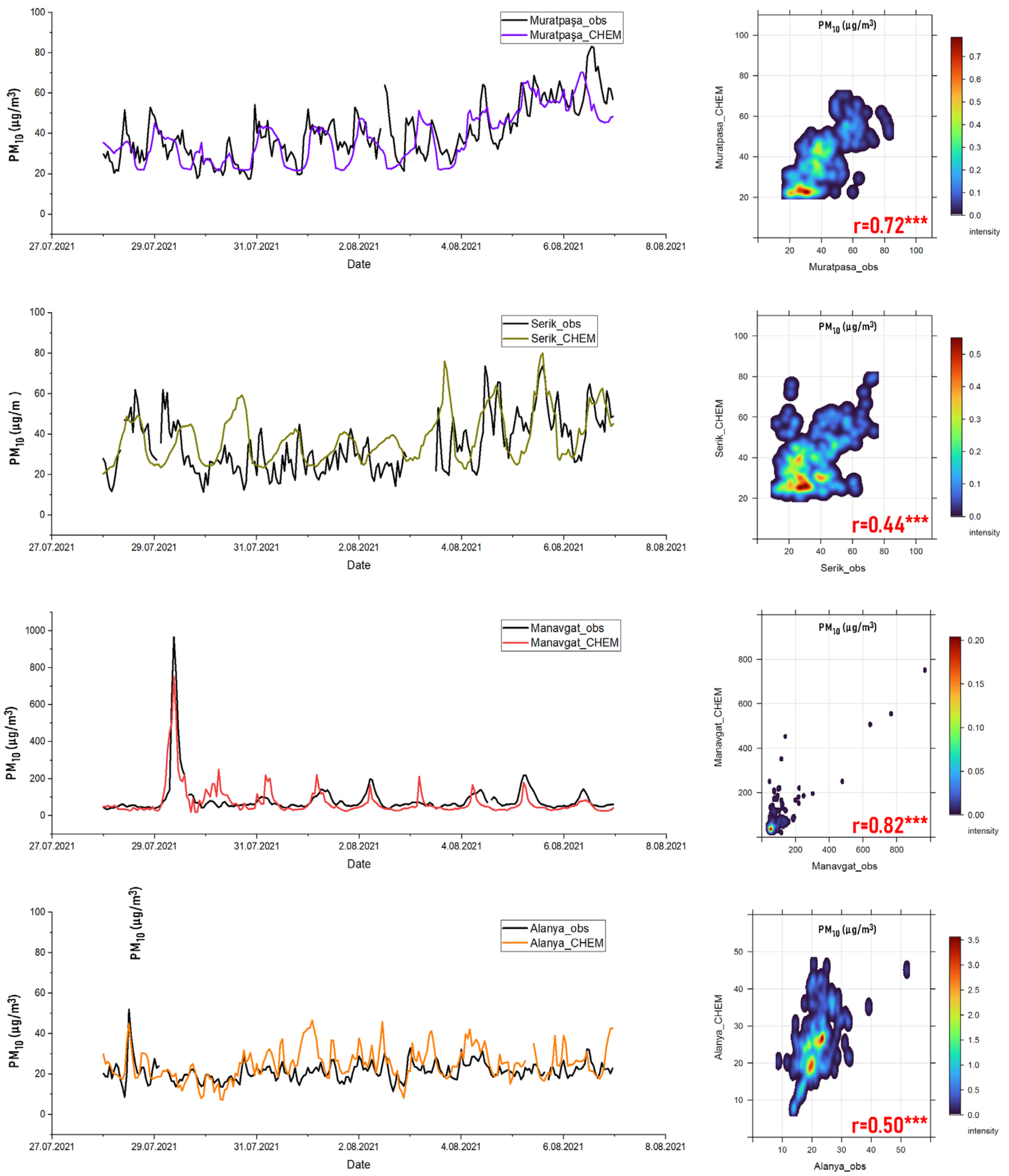

Figure 3.11 : Time series and scatter plot with a density overlay of observed and modeled PM_{10}.

3.10 Fire Plume Modelling and PM_{10} Cross Section

A comprehensive investigation of the fire plume model has unveiled critical insights into the vertical distribution and transport mechanisms of PM_{10} particles during the forest fire event. On the onset of the fire, specifically on July 28, 2021, observations revealed the initiation of the plume at approximately 80-100 meters above sea level (Figure 3.12). The intense heat emanating from the wildfire, accompanied by an ambient air temperature of 40°C, played a decisive role in shaping the vertical dispersion of PM_{10} particles. The substantial heat generated by the blaze induced thermal updrafts, characterized by the rapid ascent of heated air, effectively carrying smoke and fine particles from the fire upwards into the atmosphere.

As the fire activity diminishes and temperatures begin to decrease, the uplifted particles disperse horizontally within the atmosphere, potentially influencing air quality at upper atmospheric levels rather than at the surface. However, on July 29, a significant event transpired as air movements led to a substantial portion of PM_{10} descending to ground level. While the Chem model indicated 750.5 µg/m3, observations recorded 966.5 µg/m3 of PM_{10}, resulting in elevated particulate matter concentrations near the surface. This phenomenon was particularly pronounced during the early morning hours when lower temperatures and boundary layer conditions facilitated the retention of particles close to the ground. As temperatures rose throughout the day, reaching a peak around 14:00 LST (UTC+3), the escalation in thermal radiation and temperatures contributed to the more uniform dispersion of pollutants throughout the atmosphere (Figure 3.12). This cyclic pattern of vertical and horizontal distribution is reflected in the PM_{10} data, showcasing a notable decrease following the peak of the event, even in the subsequent days. This observation underscores the dynamic nature of pollutant dispersion during forest fire events, highlighting the importance of understanding both vertical and horizontal transport mechanisms in assessing their impact on air quality. The geographic spread of a wildfire often correlates with an escalation in the volume of fire-generated plumes discharged into the atmosphere. This relationship was particularly evident on August 2, 2021, where the wildfire's expanding area led to a heightened emission of particulates and gases. Consequently, the fire plume underwent a more extensive dispersion. Such phenomena typically arise from the fire's consumption of additional fuel sources, resulting in increased heat output and a greater production of smoke. The fusion of synoptic maps with sophisticated 3D modeling methodologies facilitated an extensive examination, uncovering that the fire plume ascended to remarkable altitudes of up to 6 kilometers. This notable elevation was not solely attributed to thermal effects but was also shaped by the existence of a dynamic low-pressure system within the atmosphere. This atmospheric system played a pivotal role in aiding the upward ascent of the plume, enabling it to attain heights ranging from approximately 5.5 to 6 kilometers above sea level (ASL) during the event.

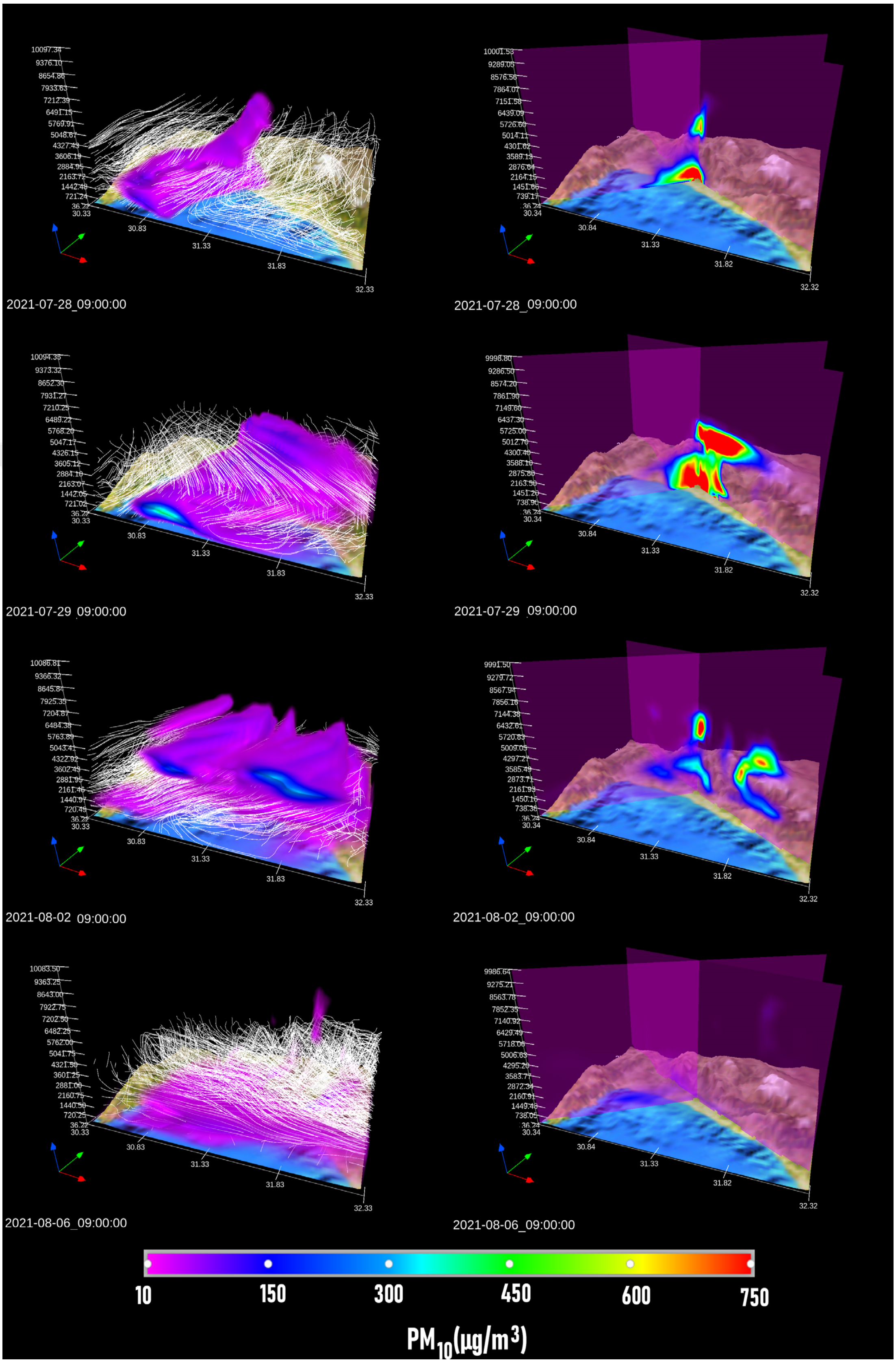

Figure 3.12 : 3D fire plume modeling with wind trajectories (right), cross section of plume with PM_{10} quantities (left).

3.11 Particulate Matter Transportation Event

The persistence of elevated aerosol levels in the eastern region of Antalya, even after local fires have been extinguished, as evidenced in satellite imagery from August 6, 2021, underscores the complex dynamics of wildfire smoke and particulate matter transport. This phenomenon suggests that following the cessation of the fires, particulate matter, including PM_{10} particles, originated not only from the local fires but also from distant sources, such as the fires in Muğla and Greece (Figure 3.13). According to the referenced Chem model, particulate matter concentrations were predicted to reach levels as high as 75.4 µg/m³, and ground-level observations recorded similar values ranging from 68.7 to 75.4 µg/m³.

Figure 3.13 : Aqua Modis Corrected reflectance imagery on 05.08.2021 and 06.08.202.

4. DISCUSSION

4.1 Meteorological Situation

Leveraging a critical examination of the outputs from the Weather Research and Forecasting (WRF) model facilitates a connection, shedding light on how overarching atmospheric patterns manifest into microscale weather events, directly impacting fire behavior. The high-resolution outputs generated by the WRF model, particularly those pertaining to temperature and relative humidity, emerge as invaluable tools for micrometeorological analysis. These outputs offer nuanced insights into the environmental conditions conducive to fire ignition and rapid spread. Notably, factors such as soaring maximum temperatures, diminished relative humidity, scant precipitation, and the velocity and orientation of local winds stand out for their pivotal roles in exacerbating fire risks. Citing recent studies by Jain et al. (2022) and Çamalan and Çamalan (2023), these factors are underscored as critical determinants in fire dynamics. However, merely acknowledging their significance is insufficient; it is imperative to assess the efficacy of the WRF model in accurately capturing these micrometeorological conditions during actual forest fire events. This evaluation involves a meticulous analysis of WRF data juxtaposed with real-time observations from ground stations within the Manavgat district. Through this comparative thesis, the model's ability to encapsulate essential micrometeorological nuances during periods of forest fires is scrutinized, offering valuable insights into its reliability and utility in predictive modeling and operational firefighting strategies.

In our examination of the Antalya Manavgat forest fires, the quantitative data extracted from the WRF-Chem model, particularly regarding the influence of the Foehn effect on temperature and relative humidity, emerge as pivotal in comprehending the fire's dynamics. The Foehn effect, distinguished by warm, arid winds, instigated significant alterations in these meteorological parameters, profoundly impacting the fire's behavior. Precisely, the WRF-Chem model data revealed that during the period influenced by the Foehn effect, temperatures in the fire-affected regions were simulated to surge noticeably, frequently surpassing 35°C. Concurrently, there was a considerable decline in relative humidity, often plummeting below 20%. Such conditions, characterized by elevated heat and diminished moisture levels, create an environment conducive to the swift propagation and escalation of wildfires.

The significance of Foehn effects in the context of forest fires stems from several key factors. These winds, renowned for their warm and arid characteristics, are a consequence of adiabatic compression as air descends the lee slopes of mountains. This process leads to a marked decrease in humidity and a simultaneous rise in temperature within the affected regions (Sharples et al., 2010). Such conditions pose a significant threat in areas susceptible to forest fires, as the amalgamation of low humidity, high temperatures, and vigorous winds can markedly intensify the strength and spread of fires, as extensively documented in the literature (Sepehri, 2022; Keikhosravi and Dizaj, 2023; Purificação et al., 2022).

4.2 PM_{10} and Aerosol Optical Depth (AOD)

In the evaluation of WRF-Chem model outputs for forest fires, numerous studies favor the integration of diverse satellite products (Reid et al., 2013; Ma et al., 2021; Jin et al., 2024). One of the most notable achievements lies in the model's remarkable prowess in forecasting Aerosol Optical Depth (AOD) with exceptional precision. This proficiency was notably evident at the Manavgat air quality and meteorological station, situated in close proximity to the fire zone. Here, the model exhibited a robust correlation coefficient of 0.93 for AOD, emphasizing its efficacy in simulating this pivotal parameter. Moreover, the investigation extended to other crucial pollutants such as the Aerosol Absorption Index (AAI) and ground-level PM_{10} concentrations. In these areas as well, the WRF-Chem model showcased considerable accuracy, with correlation coefficients of 0.81 for AAI and 0.82 for ground-level PM_{10} concentrations. These metrics highlight the model's strong predictive capacity regarding particulate pollution, shedding light on the intricate interplay between fire emissions, atmospheric dynamics, and resultant air quality. During the fire event at the Manavgat Station grid, the WRF-Chem model captured a significant Aerosol Optical Depth (AOD) range of 2.05 to 0.57, highlighting the high presence of aerosols in the atmosphere. A comparable study conducted in Greece, which shares similar geographic characteristics, revealed an AOD range of 1 to 1.54 during forest fires in August 2007 (Liu et al., 2009).

However, amid the overall success of the WRF-Chem model in forecasting key air quality indicators across most monitoring stations, its performance at the Serik meteorological station stood out for its inadequacy, particularly concerning the modeling of ground-level PM_{10} (r = 0.44) and AOD (r = 0.42). A notable issue observed at the Serik station was the near-negligible correlation with wind speed (r = 0.06), a pivotal factor crucial for accurately predicting the dispersion and concentration of aerosols. This lack of correlation with wind speed data severely impeded the model's effectiveness in precisely simulating ground-level PM_{10} and AOD at this specific location as stated San José et al. (2015). As a result, the model's projections for particulate pollution and aerosol concentration in the Serik region deviated significantly from actual observations, highlighting the inherent challenges in modeling air quality in areas where critical meteorological data correlations are weak or absent.

4.3 3D Plume Modeling

The incorporation of 3D plume modeling and cross-sectional analysis emerged as a pivotal element, particularly in addressing the discrepancies noted between Aerosol Optical Depth (AOD) and ground-level PM_{10} concentrations on specific days. These inconsistencies across most monitoring stations underscored the intricate dynamics governing aerosol dispersion across various atmospheric strata. Through the deployment of 3D plume modeling, we delved deeper into understanding how meteorological conditions, both at the surface and in the upper atmosphere, impacted aerosol dispersion patterns. The 3D plume modeling elucidated that the thermal effects induced by the intense heat from the widespread fires, coupled with the presence of a synoptic low-pressure system, significantly influenced the vertical transport of aerosols. This phenomenon is a typical occurrence in fire scenarios, where the heightened intensity of the blaze creates its own micro-scale weather system, marked by robust upward air currents (Lareau and Clements, 2017; Tory et al., 2018). This dynamic interplay facilitated the ascent of aerosols to heights of up to 6 kilometers above sea level, unveiling a crucial aspect in comprehending the disparities observed between AOD and ground-level PM_{10} measurements. While AOD provides an overview of the total column of aerosols present in the atmosphere, ground-level PM_{10} concentrations are intricately influenced by localized factors such as dispersion mechanisms, sedimentation processes, and the complex interplay between surface and upper-level wind patterns. This multifaceted interaction between atmospheric dynamics and aerosol behavior underscores the importance of integrating advanced modeling techniques like 3D plume modeling to unravel the complexities of aerosol distribution and its impact on air quality assessments (Guevara et al., 2014).

4.4 Transportation Event

In the latter stages of the Antalya Manavgat forest fire incident, our research shed light on a notable occurrence of long-distance aerosol transport originating from distant fires in Muğla (Tariq et al., 2023), Turkey, and Greece. This phenomenon significantly influenced air quality in the western regions of Antalya, particularly at the Muratpaşa and Serik stations. The validation of this phenomenon was achieved through a combination of WRF-Chem model simulations and satellite observations, both of which indicated heightened aerosol levels in these areas. These particles were subsequently conveyed across the region by atmospheric currents. This observation resonates with findings from extensive wildfire events, as documented by Hung et al. (2020), where smoke and aerosols have been observed to traverse vast distances, ranging from hundreds to even thousands of kilometers away from their original source. The repercussions of this transport on local air quality are significant. This long-range transport of aerosols to the western expanse of Antalya underscored the extensive reach of forest fires, transcending their immediate surroundings and impacting air quality in regions situated several hundred kilometers away.

5. CONCLUSIONS AND RECOMMENDATIONS

This thesis sheds light on the intricate relationship between meteorological conditions and fire behavior during the Antalya Manavgat forest fires, identifying high temperatures, low humidity, and local wind patterns, accentuated by the Foehn effect, as significant contributors to fire intensity and spread. Furthermore, rigorous evaluation underscores the Weather Research and Forecasting model coupled with Chemistry (WRF-Chem)'s capability in accurately predicting essential atmospheric parameters, with high correlation coefficients for temperature, humidity, wind speed, and atmospheric pressure across various locations validating its effectiveness. Investigating aerosol characterization methodologies, the research reveals strong correlations between model-predicted aerosol concentrations and satellite data in some locations, yet highlights disparities in local measurements, emphasizing the need for enhanced modeling techniques. Moreover, analysis of ground-level PM_{10} concentrations showcases the WRF-Chem model's ability to replicate diurnal variations and capture extreme pollution events with remarkable accuracy in certain locations, though observed disparities underscore the importance of refining aerosol dynamics representation, especially at lower altitudes. Through employing 3D fire plume modeling and wind trajectory analysis, the thesis elucidates the complex dynamics of wildfire smoke and particulate matter transport, emphasizing the significance of integrating synoptic maps with advanced modeling techniques to enhance our understanding and prediction of air quality impacts.

5.1 Meteorological Influence on Fire Behavior

The thesis not only elucidates the intricate relationship between meteorological conditions and fire behavior during the Antalya Manavgat forest fires but also delves deeper into the complex interplay of these factors. It identifies high temperatures, low humidity levels, and local wind patterns as primary drivers of fire intensity and spread. Moreover, the exacerbation of these conditions by the Foehn effect, characterized by warm and dry downslope winds, emerges as a crucial factor amplifying the fire's severity. This phenomenon not only intensifies the initial fire conditions but also influences fire spread dynamics by altering local weather patterns. By comprehensively examining these meteorological influences, the thesis provides critical insights into the multifaceted nature of wildfire behavior, underscoring the importance of considering both macro- and microscale atmospheric conditions in fire management and mitigation strategies.

5.2 Performance of WRF-Chem Model

Through a station-by-station analysis, the research meticulously assesses the Weather Research and Forecasting model coupled with Chemistry (WRF-Chem)'s performance in simulating key meteorological parameters. While overall performance remains robust, variations in correlation coefficients, particularly for parameters like wind speed, are observed across different locations. This nuanced evaluation underscores the model's adaptability and its capacity to capture localized meteorological nuances. Despite variability, the model demonstrates consistent accuracy in replicating temperature, humidity, and atmospheric pressure patterns across various stations, validating its reliability in simulating broad-scale atmospheric dynamics. This station-specific analysis not only enhances our understanding of model performance but also informs targeted improvements to further refine its predictive capabilities, ensuring its efficacy across diverse geographical contexts. Also, The thesis investigates the accuracy of aerosol characterization methodologies, comparing satellite observations with WRF-Chem model outputs. While strong correlations between model-predicted aerosol concentrations and satellite data are observed in some locations, disparities in local aerosol measurements highlight the complexity of aerosol dynamics and the need for improved modeling techniques. In addition, Analysis of ground-level PM_{10} concentrations reveals the WRF-Chem model's ability to replicate diurnal variations and capture extreme pollution events like forest fires with remarkable accuracy in certain locations. However, observed disparities emphasize the importance of refining aerosol dynamics representation to enhance model precision, particularly at lower altitudes.

5.3 Discrepancy Analysis through 3D Fire Plume Modeling

Through the utilization of advanced 3D fire plume modeling techniques alongside meticulous wind trajectory analysis, this thesis offers a comprehensive examination of the dispersion patterns of pollutants originating from the forest fire source. By elucidating both the vertical ascent and horizontal spread of emitted pollutants, the research unveils the intricate dynamics governing wildfire smoke and particulate matter transport. This multifaceted analysis not only provides valuable insights into the spatial distribution of pollutants but also sheds light on the complex interactions between atmospheric conditions and pollutant dispersion mechanisms. Moreover, the thesis emphasizes the critical role of integrating synoptic maps with sophisticated modeling techniques to enhance our understanding and prediction of air quality impacts. By bridging the gap between macroscopic atmospheric patterns and localized pollutant dispersion dynamics, this integrative approach enables a more holistic assessment of air quality implications associated with forest fires. Furthermore, by elucidating the complex interplay between atmospheric conditions, fire behavior, and pollutant transport mechanisms, this research lays the groundwork for informed decision-making processes aimed at mitigating the adverse effects of wildfires on air quality and public health.

6. REFERENCES

AFAD. (2021). Antalya Manavgat Orman Yangını-4. *Press Release*. Retrieved from: https://www.afad.gov.tr/antalya-manavgat-orman-yangini-4 [Access date: 26.09.2023]

Akıncı, H. A., & Akıncı, H. (2023). Machine learning based forest fire susceptibility assessment of Manavgat district (Antalya), Turkey. *Earth Science Informatics*, *16*(1), 397–414. https://doi.org/10.1007/s12145-023-00953-5

Analitis, A., Georgiadis, I., & Katsouyanni, K. (2012). Forest fires are associated with elevated mortality in a dense urban setting. *Occupational and Environmental Medicine*, *69*(3), 158–162. https://doi.org/10.1136/oem.2010.064238

Antalya İl Tarım ve Orman Müdürlüğü. (2023). "Antalya". Retrieved from: https://antalya.tarimorman.gov.tr/menu/60/antalya [Access date: 27.09.2023]

Antalya Valiliği. (2021). Manavgat'ta 4 Ayrı Noktada Orman Yangını Çıktı. *Press Release*. Retrieved from: http://www.antalya.gov.tr/manavgatta-4-ayri-noktada-orman-yangini-cikti [Access date: 26.09.2023]

Arikan, D., & Yildiz, F. (2023). Investigation of Antalya forest fire's impact on air quality by satellite images using Google earth engine. *Remote Sensing Applications: Society and Environment*, *29*, 100922. https://doi.org/https://doi.org/10.1016/j.rsase.2023.100922

Arikan, D., & Yildiz, F. (2023). Investigation of Antalya forest fire's impact on air quality by satellite images using Google earth engine. *Remote Sensing Applications: Society and Environment*, *29*, 100922. https://doi.org/https://doi.org/10.1016/j.rsase.2023.100922

Aydınöz, E., Gürer, K., & Toros, H. (2014). Evaluation of WRF-CHEM Model: A case study of Air Pollution Episode in Istanbul Metropolitan. *EGU General Assembly Conference Abstracts*, 9032.

Baklanov, A. (2014). Online coupled regional meteorology chemistry models in Europe: Current status and prospects. *Atmos. Chem. Phys.*, *14*, 317–398. https://doi.org/https://doi.org/10.5194/acp-14-317-2014

Bolat, İ. (2022). Orman Yangınlarının Hava Kalitesine Etkisi: Antalya Örneği. *Journal of Bartin Faculty of Forestry*, *24*(3), 651–666. https://doi.org/10.24011/barofd.1174015

Bossioli, E., Tombrou, M., Kalogiros, J., Allan, J., Bacak, A., Bezantakos, S., Biskos, G., Coe, H., Jones, B. T., Kouvarakis, G., Mihalopoulos, N., & Percival, C. J. (2016). Atmospheric composition in the Eastern Mediterranean: Influence of biomass burning during summertime using the WRF-Chem model. *Atmospheric Environment*, *132*, 317–331. https://doi.org/https://doi.org/10.1016/j.atmosenv.2016.03.011

British Columbia. (2023). "Forest Fires and Air Quality". Retrieved from: https://www2.gov.bc.ca/gov/content/environment/air-land-water/air/air-pollution/smoke-burning/forest-fires-air-quality [Access date: 26.09.2023]

Chin, M., Rood, R. B., Lin, S.-J., Müller, J.-F., & Thompson, A. M. (2000). Atmospheric sulfur cycle simulated in the global model GOCART: Model description and global properties. *Journal of Geophysical Research: Atmospheres*, *105*(D20), 24671–24687. https://doi.org/https://doi.org/10.1029/2000JD900384

EEA. (2023). Air quality in Europe 2022: "Health impacts of air pollution in Europe". Report no. 05/2022 doi: 10.2800/488115.

European Space Agency. (2021). Copernicus Sentinel-5P (processed by ESA), TROPOMI Level 2 Ultraviolet Aerosol Index products. Version 02. https://doi.org/10.5270/S5P-3dgz66p

Freitas, S. R., Longo, K. M., Alonso, M. F., Pirre, M., Marecal, V., Grell, G., Stockler, R., Mello, R. F., & Sánchez Gácita, M. (2011). PREP-CHEM-SRC – 1.0: a preprocessor of trace gas and aerosol emission fields for regional and global atmospheric chemistry models. *Geoscientific Model Development*, *4*(2), 419–433. https://doi.org/10.5194/gmd-4-419-2011

Ginoux, P., Chin, M., Tegen, I., Prospero, J. M., Holben, B., Dubovik, O., & Lin, S.-J. (2001). Sources and distributions of dust aerosols simulated with the GOCART model. *Journal of Geophysical Research: Atmospheres*, *106*(D17), 20255–20273. https://doi.org/https://doi.org/10.1029/2000JD000053

Granier, C., J.F. Lamarque, A. Mieville, J.F. Muller, J. Olivier, J. Orlando, J. Peters, G. Petron, G. Tyndall, S. Wallens. (2005). POET, a database of surface emissions of ozone precursors, available on internet at http://www.aero.jussieu.fr/projet/ACCENT/POET.php [Access date: 26.09.2023]

Grell, G. A., Peckham, S. E., Schmitz, R., McKeen, S. A., Frost, G., Skamarock, W. C., & Eder, B. (2005). Fully coupled "online" chemistry within the WRF model. *Atmospheric Environment*, *39*(37), 6957–6975. https://doi.org/https://doi.org/10.1016/j.atmosenv.2005.04.027

Grell, G. A., Peckham, S. E., Schmitz, R., McKeen, S. A., Frost, G., Skamarock, W. C., & Eder, B. (2005). Fully coupled "online" chemistry within the WRF model. *Atmospheric Environment*, *39*(37), 6957–6975. https://doi.org/https://doi.org/10.1016/j.atmosenv.2005.04.027

Guevara, M., Soret, A., Arévalo, G., Martínez, F., & Baldasano, J. M. (2014). Implementation of plume rise and its impacts on emissions and air quality modelling. Atmospheric Environment, 99, 618–629. https://doi.org/https://doi.org/10.1016/j.atmosenv.2014.10.029

Heriyanto, E., Syaufina, L., & Sobri, M. (2015). Forecasting Simulation of Smoke Dispersion from Forest and Land Fires in Indonesia. *Procedia Environmental Sciences*, *24*, 111–119. https://doi.org/https://doi.org/10.1016/j.proenv.2015.03.015

Hersbach, H., Bell, B., Berrisford, P., Biavati, G., Horányi, A., Muñoz Sabater, J., Nicolas, J., Peubey, C., Radu, R., Rozum, I., Schepers, D., Simmons, A., Soci, C., Dee, D., Thépaut, J-N. (2023): ERA5 hourly data on single levels from 1940 to present. Copernicus Climate Change Service (C3S) Climate Data Store (CDS), DOI: 10.24381/cds.adbb2d47

Hung, W., Lu, C., Shrestha, B., Lin, H., Lin, C., Grogan, D., Hong, J., Ahmadov, R., James, E., Joseph, E. (2020). The impacts of transported wildfire smoke aerosols on surface air quality in New York State: A case study in summer 2018. Atmospheric Environment, 227, 117415. https://doi.org/10.1016/j.atmosenv.2020.117415.

Ilyas, S. Z., Khattak, A. I., Nasir, S. M., Qurashi, T., & Durrani, R. (2010). Air pollution assessment in urban areas and its impact on human health in the city of Quetta, Pakistan. *Clean Technologies and Environmental Policy*, *12*(3), 291–299. https://doi.org/10.1007/s10098-009-0209-4

İşte Manavgat yangınının bilançosu: 60 bin hektar kül oldu, en az 1 milyar TL kayıp (2021). *Sözcü Gazetesi.* Retrieved from: https://www.sozcu.com.tr/2021/gundem/iste-manavgat-yangininin-bilancosu-60-bin-hektar-kul-oldu-en-az-1-milyar-tl-kayip-6581895/ [Access date 26.09.2023]

Jaafar, H., Razi, N. A., Azzeri, A., Isahak, M., & Dahlui, M. (2018). A systematic review of financial implications of air pollution on health in Asia. *Environmental Science and Pollution Research*, *25*(30), 30009–30020. https://doi.org/10.1007/s11356-018-3049-0

Jaffe, D. A., O'Neill, S. M., Larkin, N. K., Holder, A. L., Peterson, D. L., Halofsky, J. E., & Rappold, A. G. (2020). Wildfire and prescribed burning impacts on air quality in the United States. *Journal of the Air & Waste Management Association*, *70*(6), 583–615. https://doi.org/10.1080/10962247.2020.1749731

Janssens-Maenhout, G., Crippa, M., Guizzardi, D., Dentener, F., Muntean, M., Pouliot, G., Keating, T., Zhang, Q., Kurokawa, J., Wankmüller, R., van der Gon, H., Kuenen, J. J. P., Klimont, Z., Frost, G., Darras, S., Koffi, B., & Li, M. (2015). HTAP_v2.2: a mosaic of regional and global emission grid maps for 2008 and 2010 to study hemispheric transport of air pollution. *Atmospheric Chemistry and Physics*, *15*(19), 11411–11432. https://doi.org/10.5194/acp-15-11411-2015

Jiang, F., Wang, T., Wang, T., Xie, M., & Zhao, H. (2008). Numerical modeling of a continuous photochemical pollution episode in Hong Kong using WRF–chem. *Atmospheric Environment*, *42*(38), 8717–8727. https://doi.org/https://doi.org/10.1016/j.atmosenv.2008.08.034

Kabatas, B., Pierce, R. B., Unal, A., Rogal, M. J., & Lenzen, A. (2018). April 2008 Saharan dust event: Its contribution to PM_{10} concentrations over the Anatolian Peninsula and relation with synoptic conditions. *Science of The Total Environment*, *633*, 317–328. https://doi.org/https://doi.org/10.1016/j.scitotenv.2018.03.150

Kalpana, B., Aaron, C., & R, S. K. (2014). Addressing the Burden of Disease Attributable to Air Pollution in India: The Need to Integrate across Household and Ambient Air Pollution Exposures. *Environmental Health Perspectives*, *122*(1), A6–A7. https://doi.org/10.1289/ehp.1307822

Klimatoloji Şube Müdürlüğü (2014). İklim Sınıflandırmaları. Retrieved from: https://mgm.gov.tr/FILES/genel/makale/22_iklim_siniflandirmalari.pdf [Access date 27.09.2023]

Kumar, A., Jimenez, R., Belalcazar, L. C., & Roja, N. Y. (2016). Application of WRF-Chem Model to Simulate PM_{10} Concentration over Bogota. *Aerosol and Air Quality Research*, *16*(5), 1206–1221. https://doi.org/10.4209/aaqr.2015.05.0318

Laumbach, R. J., & Kipen, H. M. (2012). Respiratory health effects of air pollution: Update on biomass smoke and traffic pollution. *Journal of Allergy and Clinical Immunology*, *129*(1), 3–11. https://doi.org/10.1016/j.jaci.2011.11.021

Lelieveld, J. (2017). Clean air in the Anthropocene. *Faraday Discuss.*, *200*(0), 693–703. https://doi.org/10.1039/C7FD90032E

Lelieveld, J., Pozzer, A., Pöschl, U., Fnais, M., Haines, A., & Münzel, T. (2020). Loss of life expectancy from air pollution compared to other risk factors: a worldwide perspective. *Cardiovascular Research*, *116*(11), 1910–1917. https://doi.org/10.1093/cvr/cvaa025

Liu, Y., Kahn, R. A., Chaloulakou, A., & Koutrakis, P. (2009). Analysis of the impact of the forest fires in August 2007 on air quality of Athens using multi-sensor aerosol remote sensing data, meteorology and surface observations. Atmospheric Environment, 43(21), 3310–3318. https://doi.org/https://doi.org/10.1016/j.atmosenv.2009.04.010

Lyapustin A. & Wang. Y. (2022). MODIS Multi-Angle Implementation of Atmospheric Correct (MAIAC) Data User's Guide Retrieved from: https://lpdaac.usgs.gov/documents/1500/MCD19_User_Guide_V61.pdf [Access date 28.09.2023]

Lyapustin, A. & Wang, Y. (2015) MCD19A2 MODIS/Terra+Aqua Aerosol Optical Thickness Daily L2G Global 1km SIN Grid. NASA LP DAAC. http://doi.org/10.5067/MODIS/MCD19A2.006

Madala, S., Li, T., Salinas, S. v, & Liew, S. C. (2020). WRF-Chem Simulations of Aerosol Transport During the Attika Forest Fire Event of July 2018. *IGARSS 2020 - 2020 IEEE International Geoscience and Remote Sensing Symposium*, 5578–5580. https://doi.org/10.1109/IGARSS39084.2020.9324510

Morison J. (2023) "Forest fires and climate change". Retrieved from: https://www.forestresearch.gov.uk/research/climate-change-impacts/forest-fires-and-climate-change/ [Access date: 27.09.2023]

Mozny, M., Trnka, M., & Brázdil, R. (2021). Climate change driven changes of vegetation fires in the Czech Republic. *Theoretical and Applied Climatology*, *143*(1), 691–699. https://doi.org/10.1007/s00704-020-03443-6

Müller, J.-F., Stavrakou, T., Wallens, S., de Smedt, I., van Roozendael, M., Potosnak, M. J., Rinne, J., Munger, B., Goldstein, A., & Guenther, A. B. (2008). Global isoprene emissions estimated using MEGAN, ECMWF analyses and a detailed canopy environment model. *Atmospheric Chemistry and Physics*, *8*(5), 1329–1341. https://doi.org/10.5194/acp-8-1329-2008

NASA FIRMS. (2018). NRT VIIRS 375 m Active Fire product VJ114IMGTDL_NRT distributed from NASA FIRMS. Available on-line https://earthdata.nasa.gov/firms. doi:10.5067/FIRMS/VIIRS/VJ114IMGT_NRT.002 [Access date: 28.09.2023]

Navarro-Barboza, H., Moya-Álvarez, A., Luna, A., & Fashé-Raymundo, O. (2020). Influence evaluation of PM_{10} produced by the burning of biomass in Peru on AOD, using the WRF-Chem. *Atmósfera*, *33*(1), 71-86. Epub 04 de diciembre de 2020.https://doi.org/10.20937/atm.52711

NCAR. (2023). FINN - Fire INventory from NCAR. Retrieved from: https://www2.acom.ucar.edu/modeling/finn-fire-inventory-ncar [Access date: 27.09.2023]

Nuryanto, D. E. (2015). Simulation of Forest Fires Smoke Using WRF-Chem Model with FINN Fire Emissions in Sumatera. *Procedia Environmental Sciences*, *24*, 65–69. https://doi.org/https://doi.org/10.1016/j.proenv.2015.03.010

Powers, J. G., Klemp, J. B., Skamarock, W. C., Davis, C. A., Dudhia, J., Gill, D. O., Coen, J. L., Gochis, D. J., Ahmadov, R., Peckham, S. E., Grell, G. A., Michalakes, J., Trahan, S., Benjamin, S. G., Alexander, C. R., Dimego, G. J., Wang, W., Schwartz, C. S., Romine, G. S., … Duda, M. G. (2017). The Weather Research and Forecasting Model: Overview, System Efforts, and Future Directions. *Bulletin of the American Meteorological Society*, *98*(8), 1717–1737. https://doi.org/https://doi.org/10.1175/BAMS-D-15-00308.1

Rizza, U., Avolio, E., Morichetti, M., di Liberto, L., Bellini, A., Barnaba, F., Virgili, S., Passerini, G., & Mancinelli, E. (2023). On the Interplay between Desert Dust and Meteorology Based on WRF-Chem Simulations and Remote Sensing Observations in the Mediterranean Basin. *Remote Sensing*, *15*(2). https://doi.org/10.3390/rs15020435

Rizza, U., Miglietta, M. M., Mangia, C., Ielpo, P., Morichetti, M., Iachini, C., Virgili, S., & Passerini, G. (2018). Sensitivity of WRF-Chem model to land surface schemes: Assessment in a severe dust outbreak episode in the Central Mediterranean (Apulia Region). *Atmospheric Research*, *201*, 168–180. https://doi.org/https://doi.org/10.1016/j.atmosres.2017.10.022

Rooney, B., Wang, Y., Jiang, J. H., Zhao, B., Zeng, Z.-C., & Seinfeld, J. H. (2020). Air quality impact of the Northern California Camp Fire of November 2018. *Atmospheric Chemistry and Physics*, *20*(23), 14597–14616. https://doi.org/10.5194/acp-20-14597-2020

San José, R., Pérez, J. L., Balzarini, A., Baró, R., Curci, G., Forkel, R., Galmarini, S., Grell, G., Hirtl, M., Honzak, L., Im, U., Jiménez-Guerrero, P., Langer, M., Pirovano, G., Tuccella, P., Werhahn, J., & Žabkar, R. (2015). Sensitivity of feedback effects in CBMZ/MOSAIC chemical mechanism. Atmospheric Environment, 115, 646–656. https://doi.org/https://doi.org/10.1016/j.atmosenv.2015.04.030

Sarı, C. & Koçak, İ. (2012). Antalya'nın Genel Coğrafya Özellikleri in *Dünden Bugüne ANTALYA.* Retrieved from https://antalya.ktb.gov.tr/Eklenti/38500,2012-idundenbuguneantalya.pdf?0 [Access date: 27.09.2023]

Schroeder W. & Giglio. L. (2018). NASA VIIRS Land Science Investigator Processing System (SIPS) Visible Infrared Imaging Radiometer Suite (VIIRS) 375 m & 750 m Active Fire Products: Product User's Guide Version 1.4 .Retrieved from: https://viirsland.gsfc.nasa.gov/PDF/VIIRS_activefire_User_Guide.pdf [Access date 28.09.2023]

Schultz, M. G., Heil, A., Hoelzemann, J. J., Spessa, A., Thonicke, K., Goldammer, J. G., Held, A. C., Pereira, J. M. C., & van het Bolscher, M. (2008). Global wildland fire emissions from 1960 to 2000. *Global Biogeochemical Cycles*, *22*(2). https://doi.org/https://doi.org/10.1029/2007GB003031

Song, Q., Christiani, D. C., XiaorongWang, & Ren, J. (2014). The Global Contribution of Outdoor Air Pollution to the Incidence, Prevalence, Mortality and Hospital Admission for Chronic Obstructive Pulmonary Disease: A Systematic Review and Meta-Analysis. *International Journal of Environmental Research and Public Health*, *11*(11), 11822–11832. https://doi.org/10.3390/ijerph111111822

Spiridonov, V., Jakimovski, B., Spiridonova, I., & Pereira, G. (2019). Development of air quality forecasting system in Macedonia, based on WRF-Chem model. *Air Quality, Atmosphere & Health*, *12*(7), 825–836. https://doi.org/10.1007/s11869-019-00698-5

Tuccella, P., Curci, G., Visconti, G., Bessagnet, B., Menut, L., & Park, R. J. (2012). Modeling of gas and aerosol with WRF/Chem over Europe: Evaluation and sensitivity study. *Journal of Geophysical Research: Atmospheres*, *117*(D3). https://doi.org/https://doi.org/10.1029/2011JD016302

Turco, M., Rosa-Cánovas, J. J., Bedia, J., Jerez, S., Montávez, J. P., Llasat, M. C., & Provenzale, A. (2018). Exacerbated fires in Mediterranean Europe due to anthropogenic warming projected with non-stationary climate-fire models. *Nature Communications*, *9*(1), 3821. https://doi.org/10.1038/s41467-018-06358-z

Tariq, S., ul-Haq, Z., Mariam, A., Mehmood, U., Ahmed, W., (2023). Assessment of air quality during worst wildfires in Mugla and Antalya regions of Turkey. Natural Hazards, 115(2), 1235–1254. https://doi.org/10.1007/s11069-022-05592-5

WHO. (2014). "Air Pollution". Retrieved from: https://www.who.int/health-topics/air-pollution [Access date: 26.09.2023]

WHO. (2023). "Wildfires". Retrieved from: https://www.who.int/health-topics/wildfires [Access date: 26.09.2023]

Wiedinmyer, C., Kimura, Y., McDonald-Buller, E. C., Emmons, L. K., Buchholz, R. R., Tang, W., Seto, K., Joseph, M. B., Barsanti, K. C., Carlton, A. G., & Yokelson, R. (2023). The Fire Inventory from NCAR version 2.5: an updated global fire emissions model for climate and chemistry applications. *Geoscientific Model Development*, *16*(13), 3873–3891. https://doi.org/10.5194/gmd-16-3873-2023

Yevich, R., & Logan, J. A. (2003). An assessment of biofuel use and burning of agricultural waste in the developing world. *Global Biogeochemical Cycles*, *17*(4). https://doi.org/https://doi.org/10.1029/2002GB001952

Yienger, J. J., & Levy II, H. (1995). Empirical model of global soil-biogenic NOχ emissions. *Journal of Geophysical Research: Atmospheres*, *100*(D6), 11447–11464. https://doi.org/https://doi.org/10.1029/95JD00370

Yilmaz, O. S., Acar, U., Sanli, F. B., Gulgen, F., & Ates, A. M. (2023). Mapping burn severity and monitoring CO content in Türkiye's 2021 Wildfires, using Sentinel-2 and Sentinel-5P satellite data on the GEE platform. *Earth Science Informatics*, *16*(1), 221–240. https://doi.org/10.1007/s12145-023-00933-9

Zhou, Y., Ma, X., Tian, R., & Wang, K. (2023). Seasonal transition of Black carbon aerosols over Qinghai-Tibet Plateau: Simulations with WRF-Chem. *Atmospheric Environment*, *308*, 119866. https://doi.org/https://doi.org/10.1016/j.atmosenv.2023.119866

Zhuang, Y., Fu, R., Santer, B. D., Dickinson, R. E., & Hall, A. (2021). Quantifying contributions of natural variability and anthropogenic forcings on increased fire weather risk over the western United States. *Proceedings of the National Academy of Sciences*, *118*(45), e2111875118. https://doi.org/10.1073/pnas.2111875118

7. CURRICULUM VITAE

Name Surname : **Yiğitalp KARA**

EDUCATION :

- **B.Sc.** : 2022, Istanbul Technical University, Faculty of Aeronautics and Astronautics, Department of Meteorological Engineering

PROFESSIONAL EXPERIENCE AND REWARDS:

- 2024 Samsun University, Research Assistant
- 2023 Buluttan Weather Intelligence & Climate Adaptation, Meteorological Engineer
- 2022 Nordex Group Turkey, Wind & Site Engineering Intern
- 2021 The Scientific and Technological Research Council of Turkey**,** *Research Project Assistant*

PUBLICATIONS, PRESENTATIONS AND PATENTS ON THE THESIS:

- **Kara, Y.**, & Toros, H. (2023). ANTALYA-MANAVGAT FOREST FIRES: A WRF-CHEM AND REMOTE SENSING ANALYSIS. The Ninth International WEBIOPATR Workshop & Conference Particulate Matter: Research and Management WeBIOPATR 2023, 75. Vinča, Belgrade 2023. https://www.vin.bg.ac.rs/webiopatr/2023/wp-content/uploads/2023/12/WeBIOPATR2023_BookOfAbstracts.pdf#page=75

OTHER PUBLICATIONS, PRESENTATIONS AND PATENTS:

A. Articles published in international peer-reviewed journals

- A1. **Kara Y.**, Aydın S., Karanfil E., Özgür E. (2022). Prediction of Wind Speed by Using Chaotic Approach: A Case Study in Istanbul . International Journal of Environment and Geoinformatics , 9 (3) , 48-56 , March 2022. https://doi.org/10.30897/ijegeo.994011
- A2. Yılmaz, M., **Kara, Y.**, Çulpan, H. C., Can, G., & Toros, H. (2023). Detection and regional analysis of heatwave characteristics in İstanbul. *Sustainable Cities and Society*, *97*, 104789. https://doi.org/https://doi.org/10.1016/j.scs.2023.104789
- A3. Yılmaz, M., **Kara, Y.**, Toros, H., & İncecik, S. (2024). Analysis of the summer thermal comfort indices in İstanbul. *International Journal of Biometeorology*. https://doi.org/10.1007/s00484-024-02669-7

- A4. Ünal Z.F., **Kara Y.**, Dinç U., Öztürk R., Çöl İ., Öztürk B., Toros H., Aydın U. (2021). Lockdown effects on air pollution with meteorological conditions in Istanbul. Al'ternativnaâ ènergetika i èkologiâ (ISJAEE). 2021;(01-03):77-90. https://doi.org/10.15518/isjaee.2021.01.005

- A5. Öztürk B., Çöl İ., Öztürk R., Dinç U., **Kara Y.**, Ünal Z.F., Toros H., Aydın U. (2021). Evaluation of Istanbul Air Pollution in Combating COVID-19. Al'ternativnaâ ènergetika i èkologiâ (ISJAEE). 2021;(01-03):91-101. https://doi.org/10.15518/isjaee.2021.01.006

- A6. **Kara, Y.**, Yavuz, V., Temiz, C., & Lupo, A. R. (2024). Exploring Spatio-Temporal Precipitation Variations in Istanbul: Trends and Patterns from Five Stations across Two Continents. *Atmosphere*, *15*(5). https://doi.org/10.3390/atmos15050539

B. Papers presented at international scientific meetings and published in proceedings books

- B1. **Kara Y.**, Dinç U., Ünal Z.F. , Deniz N.G., Toros H. (2021). Performance Testing on Wind Forecasts of WRF Model with Analysis Data in Turkey. 8th International Meeting on Meteorology and Climatology of the Mediterranean, Online, 25-27 May 2021.

D. Articles published in national peer-reviewed journals

- D1. **Kara, Y.**, Dursun, Ş., Toros, H. (2020). Assessment of Air Pollution in Trabzon During COVID-19 Measures. Journal of Research in Atmospheric Science Vol. 2, No. 1, pp. 1-6, June 2020.

- D2. **Kara Y.**, Karakaya T., Pirselimoğlu G., Dursun Ş., Toros H. (2020). Overall Evaluation of NOx , NO, NO2 Gasses in Turkey and Their Data Quality Control. Journal of Research in Atmospheric Science Vol. 2, No. 1, pp. 12-16, June 2020.

- D3. **Kara, Y.**, Çivici, M. , Kartum, U. & Flores Rangel, R. M. (2022). General Assessment of PM_{10} and SO2 in Ağrı City Centre. International Journal of Advances in Engineering and Pure Sciences , 34 (1) , 38-49 . DOI: https://doi.org/10.7240/jeps.927084

E. Papers presented at national scientific meetings and published in proceedings books

- E1. **Kara Y.**, Öztopal A., Kahya C. (2019). Marmara Bölgesi İçin Uydu Verileri Kullanılarak PM_{10} Tespiti. IV. Meteorolojik Uzaktan Algılama Sempozyumu (UZALMET2019). ISBN NO: 978-605-7599-30-8(...)